

VIRGINIA DIVISION OF MINERAL RESOURCES  
OPEN-FILE REPORT 07-01

THE TECTONIC HISTORY AND CHARACTERISTICS OF  
FRACTURE SYSTEMS AFFECTING  
COAL MINE ROOF STABILITY IN  
SOUTHWEST VIRGINIA

Craig B. Byington



COMMONWEALTH OF VIRGINIA  
DEPARTMENT OF MINES, MINERALS AND ENERGY  
DIVISION OF MINERAL RESOURCES  
Edward E. Erb, State Geologist

CHARLOTTESVILLE, VIRGINIA  
2007

COVER: Roof-rock delamination along carbonaceous and micaceous micro-shear planes. Rock bolt plates for scale are 20 centimeters.

## CONTENTS

	Page
Abstract.....	1
Introduction.....	1
Acknowledgements.....	2
Regional structural setting.....	3
Virginia coalfield historical perspective.....	5
Conceptual framework for structural analysis.....	5
Methods.....	6
Structural data collection .....	6
Petrographic data collection .....	6
Stereonet data processing .....	7
Results.....	9
Deformation events general .....	11
Deformation event D1a.....	12
Deformation event D1b.....	15
Deformation event D2a – semi-ductile domain.....	18
Deformation event D2a – brittle domain.....	23
Deformation event D2b.....	27
Other tectonic-related discontinuities.....	29
Summary and conclusions .....	32
References cited.....	33

### Tables

Table	Page
I Typical fracture characteristics of Virginia’s coal mines .....	8
II Generalized deformation events and calculated stress field orientations .....	10
III Rock composition petrography .....	22
IV Spearman-rank correlation matrix of rock composition.....	24

### Illustrations

Figure	Page
1. Map of referenced coal mines in Southwest Virginia .....	3
2. Structural map of the Virginia coal fields showing major faults and folds.....	4
3. Schematic of irrotational simple shear and pure shear.....	7
4. Photomicrograph showing diagenetic minerals and tectonically reformed coal stringers.....	7
5. Stereonet plot of all planar data along State Highway 160 .....	11
6. Map showing D1 faults, D1 folds, D2 faults and D2 folds .....	12
7. Near-vertical D1b shear plane coated with re-annealed coal.....	13
8. Pound Gap fault in U.S. Highway 23 road cut .....	13
9. Black ultracataclasite injected into fractures in footwall arenite of Pound Gap fault .....	14
10. Pound Gap road cut with sulfidic arenite and tectonically injected coal .....	14
11. Arenite roof extension fractures .....	15
12. State Highway 160 road cut of arenite, graywacke and coal seam.....	16
13. Intersection of D1b fault with D2 IS shear and splay .....	16
14. Stereonet of mean stress-field orientations for sub-events D1a and D1b .....	17

15. Stereonet pole plot of cleating.....	17
16. Imboden seam with duplex sole .....	17
17. Stereonet of mean stress-field orientations for sub-events D2a and D2b .....	18
18. Coal seam showing orthomylonite shearing .....	18
19. Photomicrograph of orthomylonitic fabric in coal .....	19
20. Photomicrograph of stretched and folded cutinite macerals in coal mylonite fabric .....	19
21. Mylonite zone in arenite host .....	20
22. Three coal and mica-lined mylonite shears in State Highway 160 road cut .....	21
23. Transition from primary carbonaceous fragments to shear re-aligned coal stringers .....	21
24. Photomicrograph showing coal stringers cutting through and elongating blebs of coal .....	23
25. IS shear showing characteristic of sigmoidal shear fabric in coal .....	24
26. IS shear showing characteristic of sigmoidal shear fabric in graywacke.....	24
27. Typical appearance of LA extension fractures in roof .....	25
28. Examples of duplexed coal seams.....	26
29. IS shears characterized by narrow glide plane and no extension fractures in roof.....	26
30. IS shear splays exiting coal seam into roof strata .....	27
31. Coal stringers filling extension fractures cutting bedding .....	28
32. Coal stringers injected into sandstone host .....	28
33. Typical “horseback” fall caused by intersecting extension fractures.....	29
34. Floor buckling along LA extension fracture .....	29
35. Macro- and microscopic bands of coal micro-stringers in arenite host .....	30
36. Photomicrograph showing coal stringers from remobilized pre-existing coal blebs.....	31
37. Roof-rock delamination along carbonaceous and micaceous micro-shear planes.....	31
38. Roof fall with tabular blocks indicative of roof delamination .....	3

# The Tectonic History and Characteristics of Fracture Systems Affecting Coal Mine Roof Stability in Southwest Virginia

Craig B. Byington

## ABSTRACT

This work presents an integrated model for recognizing macroscopic and microscopic coal-mine fracture discontinuities related to coal-mine roof falls in Southwest Virginia. In addition, the regional deformation history consisting of two distinct deformation events and their associated faults, folds and fractures is defined within the context of coal-mine roof falls. The results of Stress-field Orientation Mapping and Analysis (SOMA, Byington, 2004) calculations in the coal mines, which defines the mean, operative, stress field in Southwest Virginia are also included.

The supporting database, which consists of over 13,000 rock measurements from 2,263 discontinuity sets and 30 petrographic examinations, was assembled from eight underground coal mines and several dozen highway road-cut exposures throughout the coalfield of Southwest Virginia. From this database comes new insight into the paleo-kinematics of Southwest Virginia's fault-bounded blocks. Each of the conjugate fracture sets is defined within the context of its paleo-deformation history and also in the context of its currently operative stress field.

Two deformation events, each consisting of two sub-events, produced unique sets of faults, extension fractures, riedel shears and folds. The geometries of the conjugate-fractures and their fold orientations were used to determine the paleo-stress fields and paleo-kinematics. The first event was dominated by strike-slip displacement and the second event by dip-slip displacement.

A detailed list of key characteristics is described for each fracture type within the two deformation events and photographic examples are provided. The fractures' descriptive geometries and interactions with each other are described

within the context of roof falls. A computer-aided, stereonet-based technique for organizing and interpreting important fracture sets is also reviewed.

Tectonically controlled evolution of the host rock's composition is discussed in the context of coal-mine roof falls. Transmitted-light thin-section petrography is used to identify micro-fracture discontinuities in the coal and to describe the relationships of various micro-fracture fabrics in the host rock. These micro-fabrics include mylonite, cataclasite, and tectonically induced coal stringers and mica-grain reorientations. Depending on stress-field orientations the micro-fracture fabrics can strongly influence the rock strength, cohesion, and ultimately, the probability of roof-rock failure.

## INTRODUCTION

Approximately 1,500 roof falls and between 500 and 600 roof fall injuries occur each year in the U.S. (Molinda, and others, 2000). An improved understanding of the factors involved in all types of groundfalls is required for improved safety and profitability in coal mines.

This paper is constructed to accomplish several purposes in a way that is most convenient for the reader to understand. Beginning on page three the general tectonic setting is laid out. Because few workers are familiar with the techniques for calculating paleo-kinematics and paleo-stress fields, beginning on page six the author attempts to explain the general structural concept, and establish the methods used to calculate these numbers. Results, beginning on page nine, describe the supporting observations

and calculations, and this is followed, beginning on page 12, by the calculated paleo-deformation events. Finally, with the concept and results foundation established, the main implications for roof control are discussed within their structural context beginning on page 27. All planar data is presented using “right-hand rule format (azimuthal strike given with dip direction clockwise at 90 degrees).

The stability of coal-mine roof rocks is more significantly affected by fracture discontinuities in the roof, floor and ribs than by any other single feature. Without fractures occurring as pre-existing joint sets, fault planes, planes of reduced cohesion, or as fractures related to subsequent mining, catastrophic failure of roof blocks cannot occur.

Fractures are a necessary component for catastrophic groundfalls occurring in all types of mines regardless of rock type, size or depth of excavation, ground-support methods, primary sedimentary structures or diagenetic history of the host rock. This does not imply that these other factors are not important in a successful ground-control analysis, but rather that the fractures are *the* fundamental ground-failure elements. As such, they are critical to the understanding and mitigation of roof falls. Because they behave in response to quantifiable factors, they are predictable, and therefore, controllable.

The architecture of fractures as weakness discontinuities in mine rocks is recognized as an important ground control consideration (Barton, 1976; Hoek, 2000). The predictable nature and wide vertical and horizontal distribution of fracture elements throughout the Virginia coal field suggests that a systematic study of fracture elements related to ground failures, especially roof falls, can greatly simplify the study of roof-control problems.

Currently however, the etiology of mine roof failures is more commonly described as non-prioritized combinations of characteristics such as rock composition, primary sedimentary features, jointing, faulting and host-rock diagenesis (Milici, and Gathright, 1982), or in the context of mining-induced fractures (Xu, and others,

2003, and Polysos, and others, 2003), or in the context of the proximity to fault and fold structures (Molinda and Ingram, 1989; McLoughlin, 1986, and Henika, 1994).

As part of an ongoing program by Virginia's Department of Mines Minerals and Energy to provide ground-control solutions for Virginia's mine operators, a fracture and a petrographic database were collected from dozens of highway road-cut exposures and from eight underground mines. These data represent common fracture elements found in the Dorchester #4 mine in the Imboden seam of the Middle-Pennsylvanian Wise Formation, the Apollo Mine #1 in the Splashdam seam of the Middle-Pennsylvanian Norton Formation, the Deep Mine #6 and Tiller #1 mines in the Raven seam of the Lower-Pennsylvanian Norton Formation, the Laurel Mountain and Deep Mine #10 mines in the Jawbone seam of the Lower-Pennsylvanian Norton Formation, and the VP #8 and Buchanan #1 mines in the Pocahontas #3 seam of the Lower-Pennsylvanian Pocahontas Formation (Figure 1).

A descriptive photograph-supported model listing the defining characteristics of the various fracture elements is provided to facilitate extrapolation of these key roof-control elements from mine to mine. The fracture sets are considered here less in the context of their deformational characteristics (amount of displacement or thickness of gouge zone) and more in the context of their frequency, rock-mechanics properties and orientation relative to the local operative stress field surrounding the mine workings. Specific techniques for interpreting the various fracture sets in the field, organizing the structural and geomechanical database, and processing the database using relatively inexpensive computer tools is provided.

## ACKNOWLEDGEMENTS

This author acknowledges the coal companies of Southwest Virginia for allowing SOMA analyses to be conducted within their mines. The author also wishes to thank L. N.

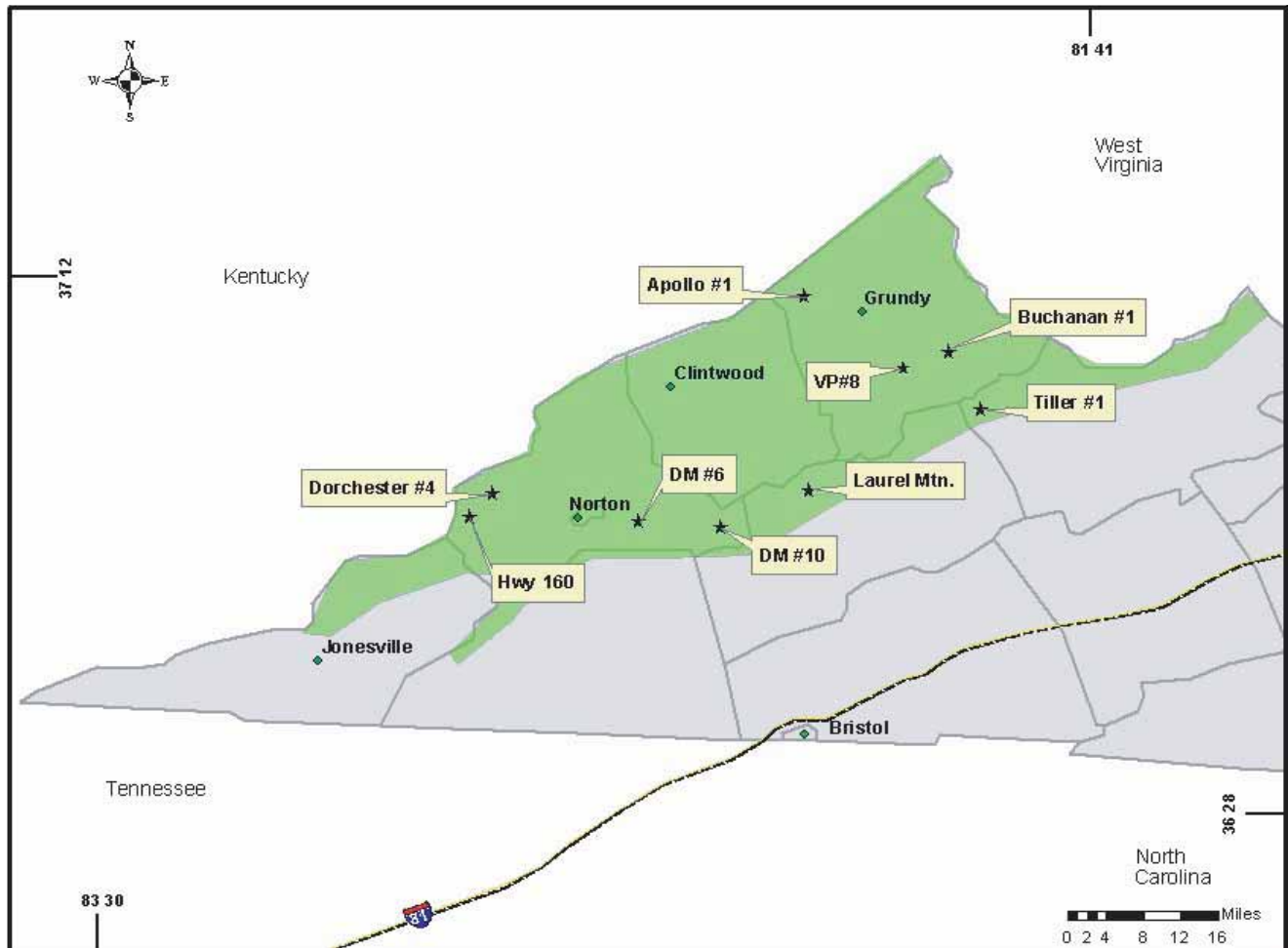


Figure 1. Counties (gray outlines) of the Southwest Virginia coalfield (green) showing location of data collection sites. Many individual highway road-cut sites are not shown.

Bright, M. Carter, W. S. Henika, T. S. Scales, M. F. Smith, A. Taylor, and R. C. Milici for their kind and useful reviews regarding this manuscript.

## REGIONAL STRUCTURAL SETTING

The study area is part of the Pine Mountain overthrust block, a complexly faulted and folded block described by various authors (for example, Milici, and Gathright, 1982; McLoughlin, 1986; and Henika, 1994) as bounded at the base by the Pine Mountain thrust-fault system, bounded on the upper surface (now eroded) by the Clinchport thrust-fault system (includes the

Clinchport, Hunter Valley, St. Paul, Buffalo Mountain, Boissevain, Copper Creek and Middle Creek faults), and cut by no less than five major transverse faults (Figure 2).

The Pine Mountain thrust-fault system surfaces in Kentucky near the border with Virginia. The sub-parallel trace of the Clinchport thrust-fault system bounds the top of the block approximately 22 miles to the south-southeast. Both fault systems generally strike N65E and dip shallowly to the southeast. During the Allegheny orogeny this overthrust block was reportedly displaced as much as 21 kilometers from the southeast to the northwest along the Pine Mountain thrust fault (Bates, 1936; Englund, 1961, and

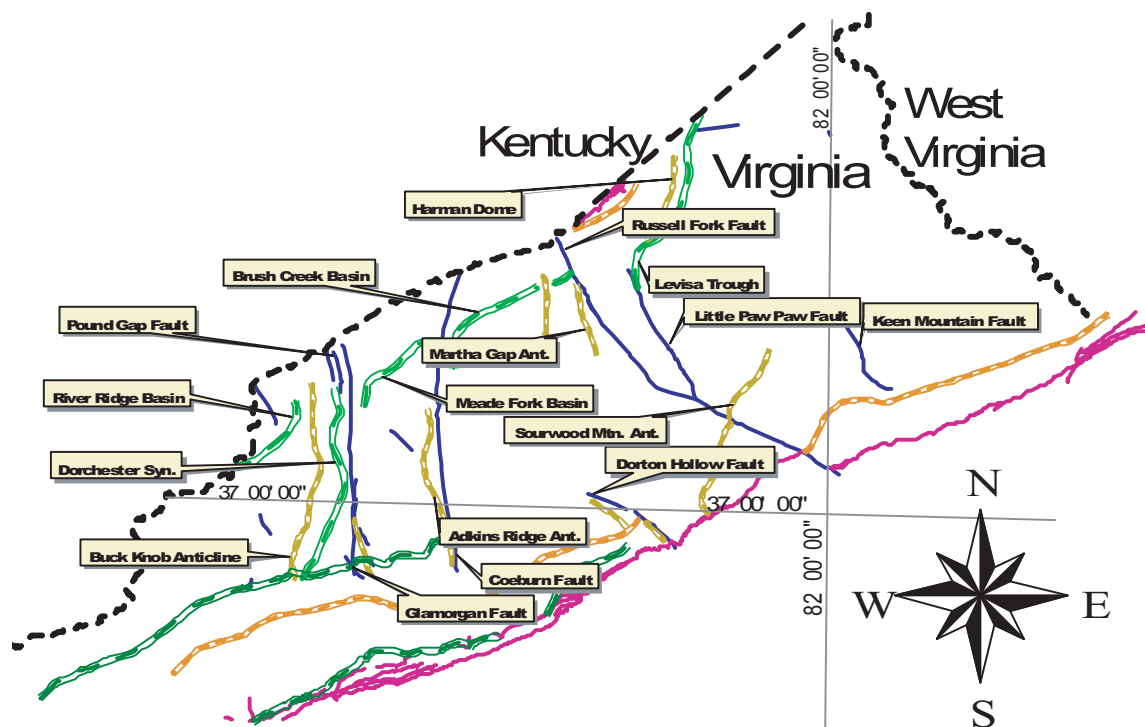


Figure 2. Structural map (not to scale) of the Southwest Virginia coalfields showing major faults (blue and purple), anticlines (tan and orange) and synclines (green) within study area (modified after Henika, 1994). Color choices are explained in text.

Henika, 1994).

The major transverse faults include the Keen Mountain, Little Paw Paw, Russell Fork, Coeburn, and Glamorgan faults. The Glamorgan and Coeburn faults strike generally N06°W with steep dips, and the southern Russell Fork and Canebrake faults strike generally N65°W also with steep dips. A number of smaller faults, including the northern end of the Russell Fork, Little Paw Paw, and Dorton Hollow faults, strike generally N35°W.

The Keen Mountain fault is described as a dextral strike-slip fault (Molinda and Ingram, 1989), and the Glamorgan fault is described as a sinistral strike-slip fault (Whitlock, and others, 1988, and Nolde, and others, 1988). The Coeburn fault is described as having 6-43 meters of displacement down to the northeast in the Caney Ridge quadrangle (Nolde, and others, 1988), and

is “believed to be strike-slip” in the Clintwood quadrangle (Difffenbach, 1988). The Russell Fork fault is described with dextral strike-slip displacement (Nolde, and others, 1984, 1988, and Henika, 1989), and the Little Paw Paw fault is also described with dextral strike-slip displacement (Nolde, and others, 1984).

Important folding includes 1) large-scale anticlines and synclines roughly paralleling and adjacent to the two major thrust-fault systems, 2) folds crossing diagonally between the north-northeast-striking transverse fault segments (Glamorgan, Coeburn and northern part of the Russell Fork faults), and 3) a few smaller folds roughly paralleling and adjacent to the northeast-striking transverse fault segments (Figure 2). The large-scale folds trend generally N61°E, and include the Middlesborough syncline, the Powell Valley anticline, the Dry Fork anticline, the North

Fork/Pigeon Creek fault/flexure, the Stone Mountain syncline, and the Pine Mountain anticline. The diagonal folds strike generally N22°E, and near the north ends of the Russell Fork, Coeburn and Glamorgan faults, they reorient the strike of bedding by approximately 40 degrees so that they trend sub-parallel to the adjacent fault to the west. The smaller folds, trending sub-parallel to the Glamorgan, Coeburn and northern part of the Russell Fork faults, strike generally N10°W and all occur in the west wall of each associated fault.

### **VIRGINIA COALFIELD HISTORICAL PERSPECTIVE**

Various authors discussing causes of Virginia coalfield roof falls have failed to agree about the priority, or even the types, of important geological features affecting coal mine roof falls. For example, Milici and Gathright (1982) described, but did not prioritize, various sedimentary characteristics of the host rock such as paleo-channels, compositional variations, rock-type boundaries, rider coal beds, soft sediment deformation and thinly bedded sandstone. They also discussed topographic features such as lineaments and structural features including folds, joints, faults, cleats, bedding-parallel faults within coal seams or in the immediate roof. Molinda and Ingram (1989), in comparison, considered bedding deformation (primarily folding) associated with large-scale faults to be the most serious ground-control element. Henika (1994), emphasized bedding-plane detachment faults as vitally important to mine safety and also transverse faults as important roof-control features.

Even when planar discontinuities (primarily fractures) are discussed in the literature, many descriptions are ambiguous or confusing. Occasionally roof fractures have been described as difficult to identify in underground mines because they are commonly closed, widely spaced and tend to be masked by other structures. Elsewhere, various planar discontinuities are confused by the use of ambiguous terms such as slips, clay

veins, hillside veins, slickensides, joint sets, or intersecting slip planes. In one description the broad generalization is made that most of the face cleats, systematic joints, fracture cleavage and faults are sub-parallel to the trend of the Powell Valley anticline, while the butt cleat, transverse joints and minor joints and faults are approximately normal to that trend. The Keen Mountain fault is ambiguously described as closely related to roof problems where displacement style varies between tensional, compressional, strike-slip shear, and fold-only displacement. In yet another description well-developed, steeply dipping, pressure-solution cleavage, reportedly related to high deviatoric stress and high hydrostatic stress, is invoked as the cause of the most prominent discontinuities along an important lineament. In no case are the genetic or geometric interrelationships of these sedimentary features, folds and fractures described, nor are they assembled into an integrated model with respect to roof control.

### **CONCEPTUAL FRAMEWORK FOR STRUCTURAL ANALYSIS**

Conjugate fractures form at predictable geometric orientations to each other and to the main shear plane as a result of stresses imposed on the rock mass (for example Cloos, 1932; McKinstry, 1948; Anderson, 1951). It is therefore possible to determine the sense of shearing along any fault by using the unique conjugate-fracture geometries, or the stress-induced fracture relationships created in the surrounding rock or developed within the gouge zone as a result of the movement along the fault plane. These sense-of-shear indicators are referred to here as kinematic indicators. Some of the most reliable and most frequently used kinematic indicators in this study include the geometric relationships of conjugate faults, fault splays, extension fractures and riedel shears found in the nearby host rock or within the fault gouge.

These conjugate-fracture geometries are utilized to define paleo-stress fields and paleo-deformation history including the paleo-kinematics. Kinematic indicators are both consistent and

predictable in their geometric relationships in any given stress field, and development of these unique fractures provides an accurate record of the paleo-stress field (McKinstry, 1948; Ragan, 1973; Twiss and Moores, 1992). Descriptions of the geometric and kinematic relationships of fracture sets for both pure and irrotational simple shear are described by various authors (Anderson, 1951; Billings, 1972; Sibson, 1977, 1989; Sylvester, 1988; Twiss and Moores, 1992). Specific examples of the principal kinematic indicators used in this study are briefly described below to illustrate the general characteristics for those unfamiliar with these relationships. Examples of applications of some of the geometric techniques employed in this report can be found in Wilcox and others (1973), Reid and others (1975), Ramsay (1980), Caddey and Byington (1988), Harding and Wickman, (1988), Byington and others (1989), Byington and Russell (2001), Byington, (2003) and Byington, (2004).

Figure 3 schematically illustrates the geometric relationship of fractures with respect to rock failure in a brittle environment (Ragan, 1973; Sylvester, 1988; Twiss and Moores, 1992). The line describing the intersection of any two types of representative conjugate fracture planes with each other or with the main shear defines the orientation of  $\sigma_2$ . The slip direction is perpendicular to that line along the plane of the main shear (Ragan, 1973). These fractals are consistent at both macroscopic and microscopic scales (for example Tchalenko, 1970).

Each distinctive deformation event results in fracture-producing rock failure or displacement within the rock body (faulting, plastic flow, folding, etc.), which is caused by a stress field unique to that deformation event (McKinstry, 1948). This stress field is commonly described with orthogonal stress vectors representing the maximum ( $\sigma_1$ ), intermediate ( $\sigma_2$ ) and minimum ( $\sigma_3$ ) principal stress orientations (Figure 3). Therefore, for a period of time each stress field in a brittle shear environment tends to open fractures approximating the  $\sigma_1$ - $\sigma_2$  (extension-fracture) plane orientation and tends to close fractures approximating the  $\sigma_2$ - $\sigma_3$  orientation

(release fracture plane). This occurs regardless of the genesis, host rock or other characteristics of the fractures; only the orientation and location with respect to the stress field are important.

## METHODS

### Structural Data Collection

Fracture data and rock specimens were collected from underground mines and from road-cut exposures in Buchanan, Dickenson, Russell, Tazewell and Wise counties. This database includes characteristics such as fracture orientations, relative fracture cohesion and friction angles, the frequency and continuity of fractures, fracture types, geometric fracture associations, crosscutting relationships, fracture-filling materials, and, for the underground exposures only, the width of fracture openings (Table I). Structural terminology, if not herein defined, follows the suggested terms defined by Wise and others (1984).

Local structural and fracture-filling characteristics reflect the general timing and geometric relationships. Kinematic indicators such as slickenside fabrics, marker-bed offsets, and many more of those described by Sibson (1989), were occasionally noted, but these were not used in computing the paleo-stress field or paleo-kinematics (Table II). For processing purposes the data were grouped according to fracture type, crosscutting relationships and permissible geometric relationships (see predicted angular relationships Figure 3).

### Petrographic Data Collection

Thirty coal and host-rock petrographic specimens were collected for thin-section analysis from within or near the coal seam, fault or fracture zone. Preparation was completed by a commercial laboratory where all thin sections were impregnated with blue epoxy, and then examined by the author using an Olympus BH2 petrographic microscope. The blue epoxy high-

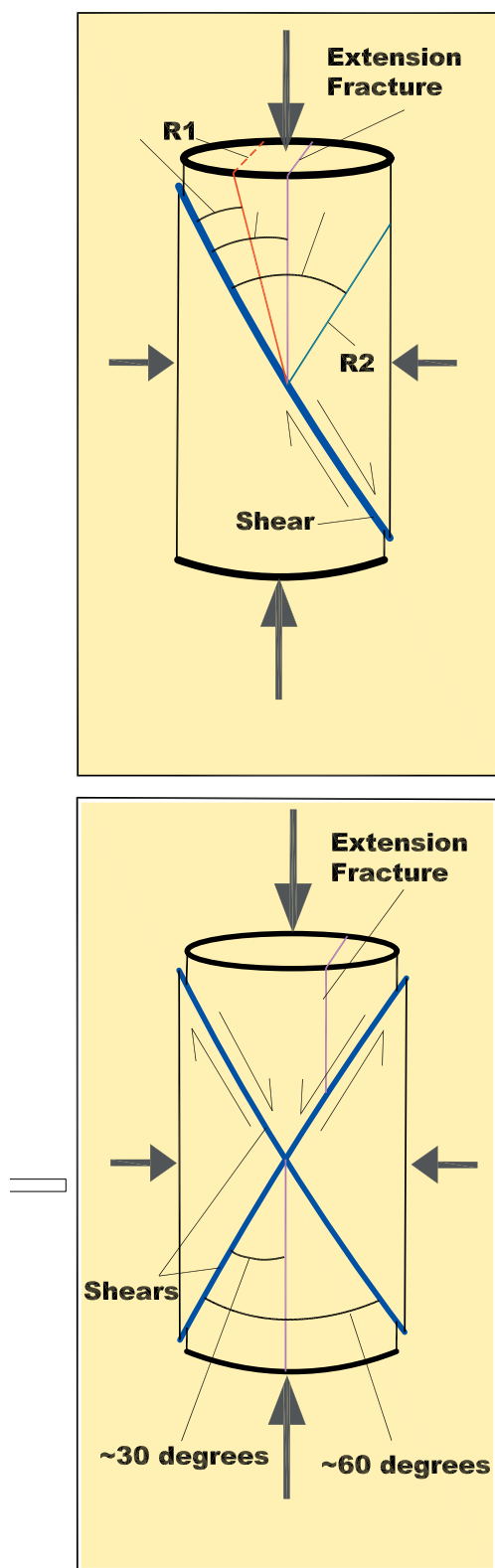


Figure 3. Schematic of pure shear at low-confining pressure (top) and high confining pressure (bottom) showing angular relationships (modified from Ragan, 1973; Sylvester, 1988; Twiss and Moores, 1992). Riedel shear planes in the simple-shear diagram are shown as R1 and R2.

lights the micro-fractures present in the sections. Care was taken to avoid the introduction of fracture artifacts as a result of the preparation process.

The composition (for example, see Figure 4) of all non-coal thin sections were quantified by completing no less than 300 point counts per thin section. The number of point counts, and the composition described as the percentage of quartz, mica, potassium feldspar, plagioclase feldspar, calcite (primarily as cement), siderite, matrix clay, hydrocarbon in stringers, hydrocarbon in blebs, and matrix are listed in Table III. Rock name assignments were made on this basis.

### Stereonet Data Processing

Structural data were processed using the DIPS © stereonet program (Diederichs and Hoek, 1998). All pole data described herein are projected on a lower hemisphere, equal-area stereonet, and all contouring was completed using the Fisher-distribution contouring method of spherical statistics included as part of the DIPS © software. No angle-bias correction (Terzaghi correction) was applied to any of the fracture or

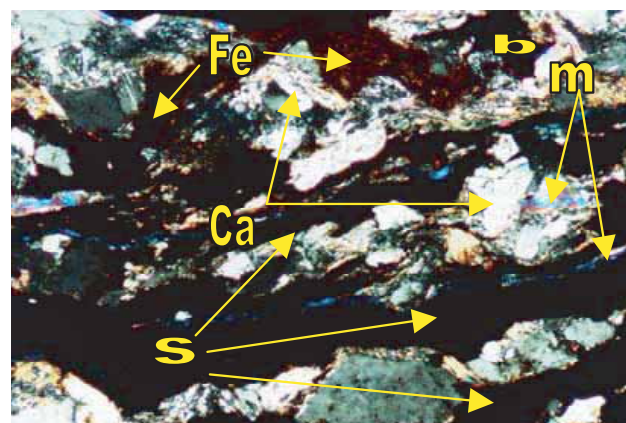


Figure 4. Transmitted light photomicrograph (crossed polarizer, 0.35 mm field of view) of sandstone in Tiller #1 mine showing calcite cement (Ca), siderite (Fe), realigned mica (m), primary coal blebs (b), and coal stringers (s).

Table I. Typical fracture characteristics of Virginia's coal mines (organized for ease of comparison of individual fracture types). LA = low-dip angle; HA= high-dip angle

Set	Fracture Type	Fracture Shape (1)	Inclination ° (2)	Filling Material (3)	Surface/ Internal Texture (4)
HA	Strike-slip (SS) fault	curviplanar (change along strike at shear to extension inflections)	near 80	rock gouge or local polished coal coat	slickensides, mullions, broad to tight core zone of deformation
LA	Dip-slip (DS) cataclastic IS shear	planar to weakly curviplanar	near 5	fine gouge to slickensided coal lenses	sigmoidal shear fabric, narrow but friable core zone of deformation
LA	Mylonitic intra-seam shear	Non-fracture	near 5	Non-fracture	reannealed with strong mylonitic fabric
LA	Splay fault (DS)	planar to strongly curviplanar	~5-45	"rider" coal seam or rock gouge	coal-polished slickensides
HA	Extension fractures (SS)	planar to rarely curviplanar	> 60	none or light clay dusting	hackly to irregular
LA	Extension fractures (DS)	planar (old) to curviplanar (new)	~ 20-35	none, clay or coal-coated slickenside	hackly (new) to polished (old)
LA	Riedel shears	curviplanar	~ 10-55	none or clay dusting	smooth, optically aligned clay coating
HA	Cleating	planar	80-85	chalcedony, limonite or calcite dusting	smooth and usually clean
LA	Bedding delaminations	planar to weakly curviplanar	near 5	coal stringer or reoriented mica	hackly to irregular

Table I, continued

Set	Fracture Type	Fracture geometry/ displacement (5)	Location (6)	Dangerous angle of fracture to $\sigma_{10}$	Distinguishing Features (category #)
HA	Strike-slip (SS) fault	~30° to HA extension fractures/ sinistral or dextral (see text)	outside of seam or merge with intra-seam shear	vertical or parallel to strike	(1), (2), (3), (4), (5), (6)
LA	Dip-slip (DS) Cataclastic IS shear	~30° to LA extension fractures/ normal or reverse (see text)	in seam or at contacts with seam	near horizontal	(1), (2), (3), (4), (5), (6)
LA	Mylonitic intra-seam shear	not determined	in seam	N/A	(4)
LA	Splay fault (DS)	~15-50° intra-seam shear/ normal or reverse	cuts bedding near seam	near horizontal	(2), (4), (5), (6)
HA	Extension fractures (SS)	~30° to strike-slip fault/ very minor to none	outside seam near HA fault	vertical or parallel to strike	(2), (3), (4), (5), (6)
LA	Extension fractures (DS)	~30° to dip-slip fault/ very minor to none	in immediate roof or inside of seam	near horizontal	(2), (3), (4), (5), (6)
LA	Riedel shears	15-30° to dip-slip fault/ minor reverse	in seam	horizontal or rarely vertical	(1), (2), (4), (5), (6)
HA	Cleating	one or two sets orthogonal to bedding/ none	in seam	vertical or parallel to strike	(1), (2), (4), (5), (6)
LA	Bedding delaminations	parallel to bedding/ none	host rock	near horizontal	(1), (2), (3), (5), (6)

fault subsets. Mean orientations for fracture sets were uniformly calculated on the stereonet by selecting poles lying within the greater-than 5% contour.

Data collected within the mines were used to compute the paleo-stress field for each deformation event (after Byington, 2003), and the mean, operative, stress field for each mine (after Byington, 2004). Comparing and contrasting the calculated paleo-stress-field orientation for each site-specific data subset was done to help confirm or disallow an assignment into one of two deformation events.

## RESULTS

As a result of the processing as described above, two distinct deformation events were revealed through analysis of the fracture database. The first deformation event (D1) is dominated by sinistral, strike-slip faulting, although later dextral displacement is also significant. This event may be related to related to early detachment along the Chattanooga decollement (Henika, 2005, personal communication). The faults and conjugate fractures associated with event D1 all have high-dip angles (the HA set).

The HA fracture data were collected along surface exposures primarily from near the trace of the Pound Gap, Glamorgan and Coeburn faults, and from underground exposures in the Deep Mine #6 mine along un-named near-north-striking D1 faults. The calculated kinematics of the principal fault plane are shown for the initial deformation event and for each subsequent event as well. The fracture geometries and timing relationships recorded in the rocks clearly indicate that event D1 is dominated by strike-slip kinematics. These calculated kinematics compare favorably to mapped offsets described by various authors (Bates, 1936; Englund, 1961; Nolde and others, 1984, 1988; Diffenbach, 1988; Whitlock and others, 1988; and Henika, 1989) for each of these faults, although the paleo-kinematics and paleo-stress field orientations shown in Table II were derived strictly from the geometric relationships of the conjugate fractures.

The second deformation event (D2) fractures are well represented in all underground and surface exposures. The D2 event is dominated by thrust faulting, although a later, relaxation-related, normal component is also well represented. The faults and conjugate fractures associated with event D2 all have low-dip angles (the LA set). The LA thrust faults, commonly found within or at the contacts of the coal seams, are responsible for the most widespread and important fracture groups with respect to roof falls. The thrust faults and their associated splays, riedel shears, extension fractures and folds interact with and offset the earlier HA faults.

The HA set produced cataclasite gouge along with near-horizontal striations and mullions, whereas the LA set developed both early mylonite and later cataclasite features. The considerable variation in mylonitic versus cataclastic deformation in the LA set suggests a deformation history that extended over a large range of temperatures, and/or displacement-versus-recovery rates.

Locally, the LA fractures radically alter the thickness and profitability of the coal seams. Where splays of the intra-seam shears locally exit the seam and enter the roof strata, they abruptly reorient bedding, alter the general composition and physical properties of the roof rock, and typically cause a significant decrease in the mine roof stability. Intersecting extension fractures, resulting from reverse and normal paleo-kinematics, cut bedding at acute angles, and are directly involved in most of the roof falls (reference Figure 3).

Photomicrographs of arenite and graywacke (after Dott, 1964) document a diagenetic sequence (Figure 4) beginning with the introduction of an early, ubiquitous calcite as cement. After fracturing, calcite and many of the silicate framework grains were locally replaced by micro-fracture-controlled siderite. Following siderite replacement, both the arenites and graywackes were refractured and cut by narrow, anastomosing swarms of micro-fracture stringers that were filled with coal or anthraxolite.

As discussed in Methods, all conjugate

Table II. Generalized deformation events and calculated paleo-stress field orientations (database consists of over 13,000 measurements from 2,263 fracture sets).

Event - D1	D1a	D1a	D1a	D1b	D1b	D1b
<b>Stress-field axes</b>	$\sigma_1$	$\sigma_2$	$\sigma_3$	$\sigma_1$	$\sigma_2$	$\sigma_3$
<b>Trend and plunge *</b>	315°, 11°	185°, 73°	047°, 13°	303°, 16°	115°, 74°	212°, 03°
<b>Mean fault strike and dip (right-hand rule)</b>	169°, 79°			358°, 70°		
<b>Kinematics D1a fault</b>	Sinistral (reverse)			Reactivated as sinistral reverse		
<b>Kinematics D1b fault</b>	N/A			Normal sinistral		

Event - D2	D2a	D2a	D2a	D2b	D2b	D2b
<b>Stress-field axes</b>	$\sigma_1$	$\sigma_2$	$\sigma_3$	$\sigma_1$	$\sigma_2$	$\sigma_3$
<b>Trend and plunge *</b>	155°, 29°	244°, 1°	336°, 61°	346°, 28°	256°, 00°	166°, 62°
<b>Mean fault strike and dip</b>	near horizontal			near horizontal		
<b>Kinematics D1a fault</b>	Reactivated as sinistral (normal)			Reactivated as dextral (normal)		
<b>Kinematics D1b fault</b>	Reactivated as sinistral (reverse)			Reactivated as sinistral (normal)		
<b>Kinematics D2a &amp; b fault</b>	Reverse			Normal		

Event - Current	Current	Current	Current
<b>Operative Stress-field axes</b>	$\sigma_{10}$	$\sigma_{20}$	$\sigma_{30}$
<b>Trend and plunge **</b>	074°, 5°	344°, 2°	231°, 84°

Orientations of stress-field vectors are listed as azimuthal bearing followed by plunge to loci of respective vector (lower hemisphere).

\* Mean calculated from all surface and underground data.

\*\* Mean calculated from underground mine data only.

fractures, when segregated into groups of like type and timing, maintain comparable structural characteristics, crosscutting relationships, geometry, and paleo-stress field orientations. Each fracture type exhibits distinct features that allow them to be identified and segregated based on those specific characteristics. Table I provides six categories for identifying the various fracture types with the more important distinguishing features being highlighted. The fractures in Table I are segregated into types found within discrete conjugate groups (HA and LA sets). These include strike-slip (HA) and dip-slip (LA) faults, mylonites (LA), extension fractures (both HA and LA), riedel shears (dominantly LA), cleating (dominantly HA) and bedding delaminations (dominantly LA). Additional categories of dis-

tinguishing characteristics applied to field data such as fracture shape, inclination, fracture-filling material, surface texture, fracture geometry, and location are listed in their order of importance with respect to characterizing individual fractures.

As defined by Byington (2004), “fracture discontinuities within a rock mass, either as pre-existing natural fractures or as mining-induced fractures, are uniquely necessary for every brittle-deformation ground failure including roof falls. The loss of, or alternatively the increase of, cohesion and associated ease of shearing along roof, rib and floor fractures reflects the interaction between the fractures and the operative stress field surrounding the mine excavation. Therefore, prediction and mitigation of roof falls

require quantifying the interaction between the fracture sets and the operative principal-compressive-stress orientation ( $\sigma_{10}$ ). This  $\sigma_{10}$  is the excavation-caused reorientation of the pre-mining  $\sigma_1$ . Since the potential for involvement in a fall also depends on the fracture's orientation with respect to the  $\sigma_{10}$ , the more dangerous orientations for each fracture type are prioritized in Table 1.

The tendency for various fracture types to cluster as discrete groups is characteristic of both underground and surface exposures throughout Southwest Virginia. For example, the segregation of fracture-types by orientation is evident in the State Highway 160 road-cut outcrops west of the city of Appalachia where the poles for the various fracture types are distinctly grouped (Figure 5).

There is also clear separation between the HA set and the LA set. These sets are represented by poles plotting near the perimeter of the stereonet for the HA set, and clustering near the center of the stereonet for the LA set (Figure 5).

### Deformation Events - General

Each set of conjugate fractures was segregated as described above using the technique described by Byington and Russell (2001) and Byington (2003), and the paleo-stress fields and main-shear kinematics were calculated. Two distinct deformation events (D1 and D2), each with two sub-events ("a" and "b"), were defined, and the calculated paleo-orientations for  $\sigma_1$ ,  $\sigma_2$  and  $\sigma_3$  are shown along with the mean orientation for each event's principal fault plane (Table II).

The faults and folds recognized during mapping by various authors and compiled by Henika (1994, plates 6a and 6b) were separated into discrete structural domains in this study. Two structural domains were defined based upon permissible conjugate fault and fold orientations, kinematics and calculated stress orientations (after Byington, 2003). Figure 6a illustrates the major D1 faults consistent in orientation with those generated during sub-event D1a. These faults and their conjugate fractures were reactivated during

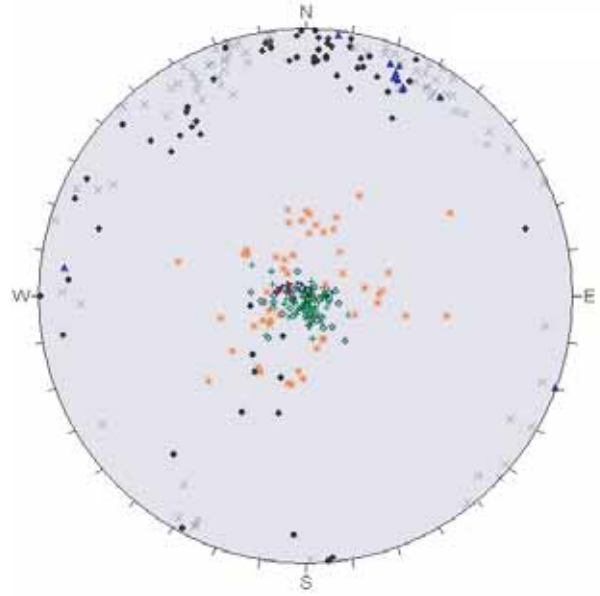


Figure 5. Stereonet plot of pole to planar data along State Highway 160 (n = 652). Faults (blue triangle), bedding (green cross), extension fractures (black dot), cleating (gray X), low-angle splay faults (light green diamond), riedel shears (orange asterisk) and intra-seam shears (red triangle) are plotted as poles.

subsequent sub-events D1b, D2a and D2b. Figure 6b illustrates the surface traces of those faults believed likely to have been generated during event D2a and reactivated during event D2b. Figure 6c illustrates the folds likely to have been generated during D1 and Figure 6d illustrates the folds likely to have been generated during event D2.

The documented folding (Figures 6c and 6d) is consistent with the maximum compressive stress paleo-directions predicted for each event (note that the orientation of  $\sigma_1$  is similar in events D1a and D1b, see Table II). Folding, developed during event D1 (Figure 6c), follows the type and orientation associated with strike-slip faulting as predicted by Sylvester (1988) and Harding and Lowell (1979). In their models the fold axis wraps from near perpendicular to the strike of the faults in locations distal to the fault trace to an axis orientation approaching parallel to the strike in proximal locations to these transverse faults (compare Figures 6a and 6b).

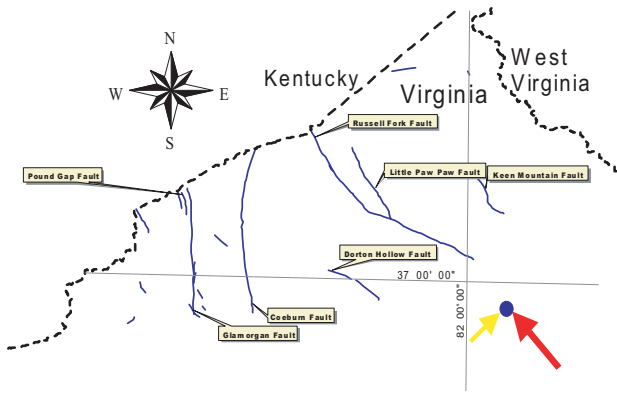


Figure 6a. Map showing D1 Faults (blue) and paleo stress field ( $\sigma_1$  = red arrow,  $\sigma_2$  = blue arrow, and  $\sigma_3$  = yellow arrow). Steep-plunging  $\sigma_2$  = strike-slip dominated faulting. Modified from Henika (1994).

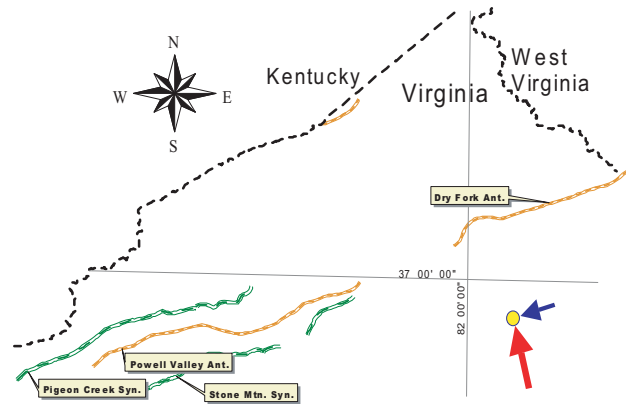


Figure 6d. Map showing D2 anticlines (golden) and synclines (green). Steep-plunging  $\sigma_3$  = reverse related folding. Modified from Henika (1994).

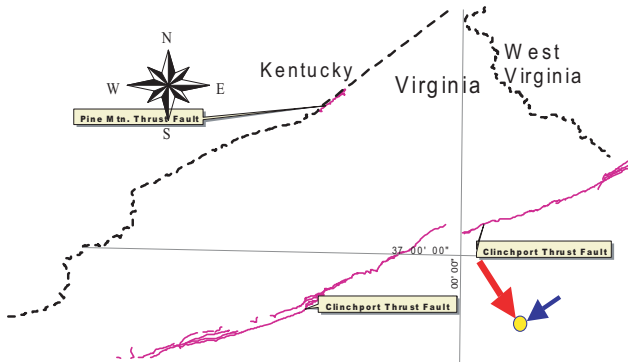


Figure 6b. Map showing D2 Faults (purple). Steep-plunging  $\sigma_3$  = reverse dominated faulting. Modified from Henika (1994).

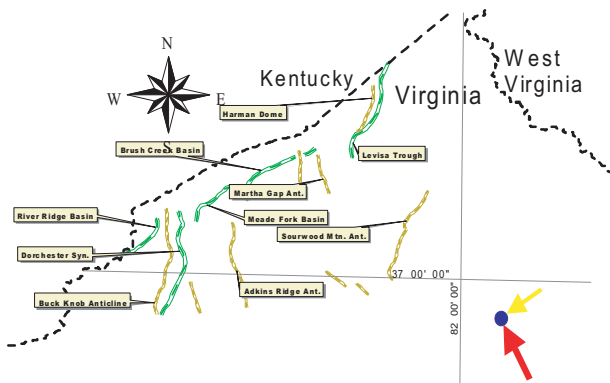


Figure 6c. Map showing D1 anticlines (golden) and synclines (green). Steep-plunging  $\sigma_2$  = strike-slip related folding. Modified from Henika (1994).

As was approximately the case with event D2, the fold axis in a thrust environment is expected to be nearly perpendicular to the  $\sigma_1$  axis. This is consistent with the folds included in event D2 (Figure 6d).

### Deformation Event D1a

Two sub-events were recognized in the first deformation event (D1a and D1b, Table II). Both D1a and D1b fracture sets strike north-northwest to north-northeast and dip steeply. Their conjugate fracture sets include riedel shears, extension fractures and release fractures. The fractures associated with the D1 event are notable as potential components of roof-falls.

The D1 faults are steeply dipping and typically exhibit well-developed sub-horizontal striations (Figure 7). The striated surface is typically well polished and coated with re-annealed coal, or white calcite. Commonly, short-wavelength folding is conspicuous in one wall, or locally, there may be crushed host rock between duplexed splays of the fault plane.

These faults, although typically characterized by kinematic indicators suggesting relatively large amounts of movement (Engelder, 1974), are commonly abruptly terminated and offset by later D2 faults.



Figure 7. Near-vertical D1b shear plane coated with re-annealed coal (Deep Mine #6 mine). Note horizontal slickenside.

The earliest sub-event recognized (D1a) has a steeply inclined ( $73^\circ$ )  $\sigma_2$  axis with associated shallowly inclined  $\sigma_1$  and  $\sigma_3$  axes. This stress field orientation is consistent with strike-slip kinematics where event D1a is characterized by sinistral strike-slip displacement with a minor reverse component. Non-folded sub-event D1a faults strike north-northwest and dip steeply southwest, and the conjugate extension fractures strike to the northwest and also dip steeply.

The complex deformational history of the D1a faults is characterized by the Pound Gap fault (Figure 8). Where the Pound Gap fault is exposed in a U. S. Highway 23 road cut at the Virginia-Kentucky border, the gouge on the foot-wall side of the core deformation zone consists of fragments of light brown, arenite-rich cataclasite intermixed with a black, ultracataclasite matrix (Figure 8 upper). A core of silica re-annealed cataclasite separates the black gouge from the crushed, green, graywacke, hanging-wall gouge. Local faint riedel shears, documenting latest reverse displacement, are preserved in the hanging wall gouge (Figure 8 lower). These three distinct types of gouge suggest at least three different displacement episodes along this fault.

Within or near the core deformation zone,

black, sandy and clayey cataclasite was injected into fractures in the arenite (Figure 9) or occurs as a hard, polished coating on the arenite fragments. The clay injections are late in timing and their geometry reflects right-lateral strike-slip (dextral) normal kinematics consistent with the calculated reactivation kinematics for event D2b

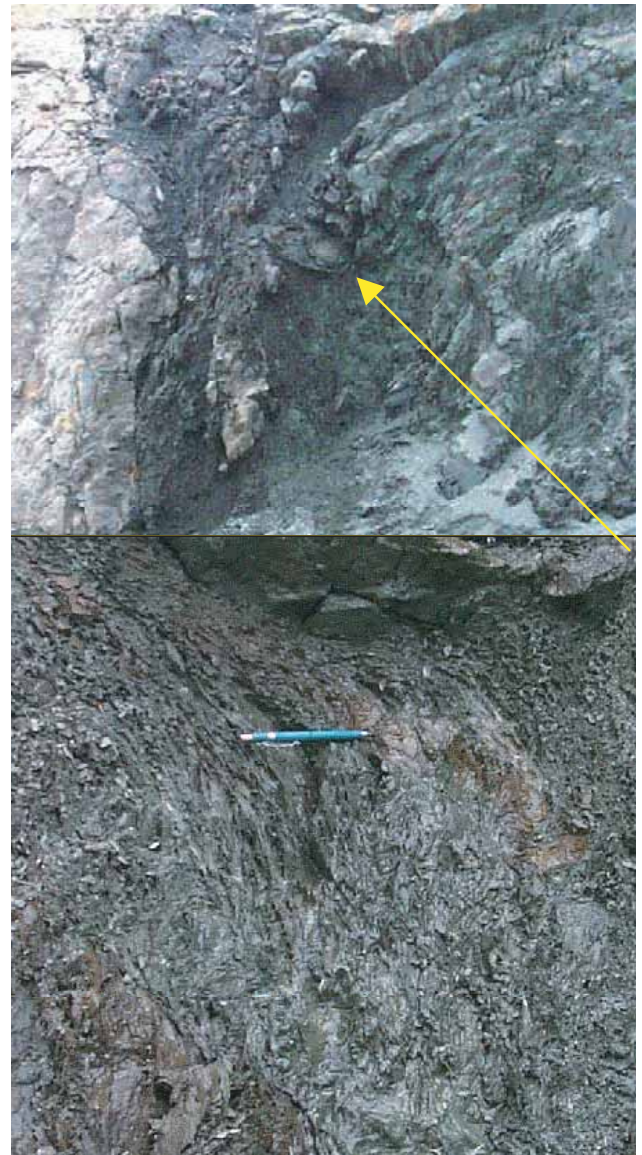


Figure 8. Pound Gap fault. **Upper** – Highway 23 road cut (4-meter field of view) showing clayey gouge (dark gray) separating arenite footwall (light brown) and shale hanging wall (green). **Lower** – close-up of gouge showing remnant riedel shears (faint, down-to-right linears, at left pencil tip) recording latest reverse displacement.



Figure 9. Black ultracataclasite injected into fractures (parallel to head of hammer) in footwall arenite of Pound Gap fault.

(Table II). The hanging-wall rock consists of interlayered, green, gray and grayish-purple graywacke and light brown, sandstone beds. Hanging-wall beds within a couple of meters of the fault are complexly folded with broad drag folds, and, where directly adjacent to the core deformation zone, tight kink banding dominates.

Several geometrically distinct sets of riedel shears, present in the black footwall gouge and green, hanging-wall gouge (Figure 8 lower), also document a complex deformational history. The footwall contains coarse, poorly milled and poorly sorted arenite gouge that is re-annealed with early silica and late calcite stringers. In contrast, the hanging-wall segment of the core deformation zone consists of milled-shale gouge with locally intense kink folding. Riedel shears (Sylvester, 1988) exhibiting strike-slip kinematics cut through the highly fractured, fissile shale in the core deformation zone, and, where blocks were locally protected from subsequent deformation, riedel shears record late reverse displacement, probably associated with D2 reactivation (Figure 8 lower).

As suggested by the complex field associations, the deformational history of the Pound Gap fault is complex. In addition the fluid epigenesis is also complex where, for example, one set of footwall extension fractures and their associated micro-fracture networks contain fine-grained, sulfide-rich fracture coatings and disseminated

pyrite halos for as much as 20 meters from the main fault conduit. There are strong sulfide disseminations within and along a well-developed, 358, 81, splay fault located in the footwall of the Pound Gap fault. The orientation and other kinematic indicators associated with this fault characterize it as resulting from a D2b-reactivation of the Pound Gap fault. This suggests that sulfide-depositing fluids were migrating upward from depth along this fault/conduit during the latest dextral/normal reactivation.

In addition, well-annealed coal-injection stringers cut through bedding of the footwall host rock. These stringers cut well-bedded arenite that contains coarse, white, well-rounded, quartz-pebble-conglomerate lenses (Figure 10). These injection stringers bend as much as 85° from orientations sub-parallel to bedding toward orientations nearly perpendicular to bedding in less than a meter.

Fracture swarms consisting of up to hundreds of often very subtle HA extension fractures are typical near the core deformation zones of D1-type faults (Figure 11). These extension fractures are typically sub-parallel in strike and dip with respect to each other although they may



Figure 10. Pound Gap road cut (8-meter-wide view) of sulfidic arenite with coal injections adjacent to the Pound Gap fault. Visual identification suggests greenish and brown hues result from oxidation of disseminated sulfides to jarosite, and to limonite (dominantly goethite), respectively. Black coal injections cut sandstone bedding (cyan line upper-right quadrant) and conglomerate lenses (yellow lines) at high angles.

occur as weakly anastomosing sets. Typically they exhibit steep dips similar to their conjugate faults, but their strikes vary by approximately  $30^\circ$  from that of their conjugate faults (see Figure 3). The HA extension fractures are typically weakly polished to coarsely irregular, commonly with large surface asperities. They occasionally contain fracture fillings such as clay, coal or calcite.

The HA extension fractures, when found alone, are rarely a significant roof-control factor because they are typically nearly perpendicular in orientation to the typical  $\sigma_{10}$  (see Table II), and as such, these fractures are rarely open. As a result of the tight closure, they are commonly rather subtle where found crossing the mine roof and can be easily missed during a roof inspection. However, when a combination of HA and

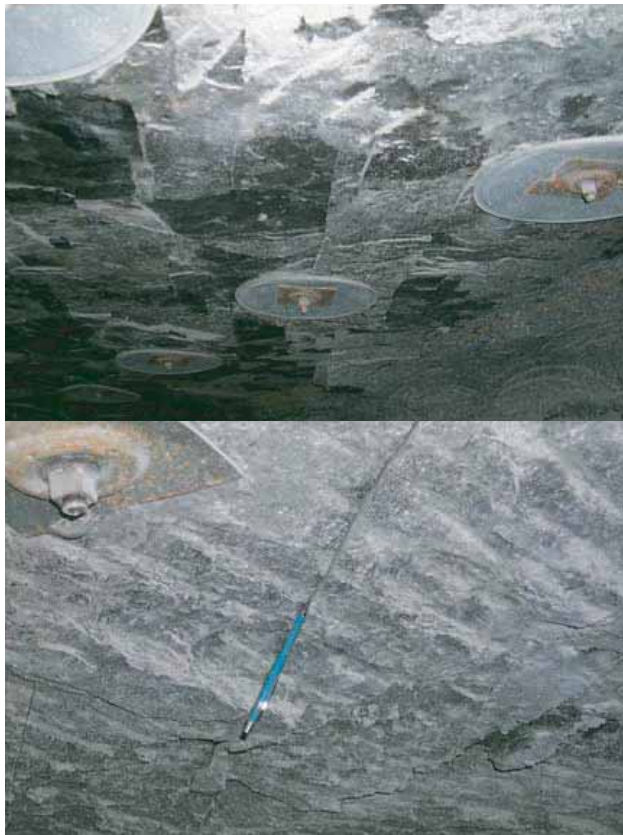


Figure 11. Roof extension fractures (Deep Mine #10 mine). **Upper** - swarm of HA extension fractures (striking directly away from viewer), and **lower** - single HA fracture (inserted pencil is 1 centimeter in diameter) of type involved with roof falls.

LA fracture sets are present these HA extension fractures play a very important role in roof falls.

Commonly, where the HA extension fractures occur near the surface, and especially where their strike approaches  $74^\circ$  ( $\sigma_{10}$ , Table I), they act as conduits for meteoric fluids. These near-surface conduits are characterized by argillic alteration and decalcification of the diagenetic carbonate cement. The resulting high-angle sandy or clayey “seams” commonly have liesegang banding. Frequently these zones are called hill seams by other authors (for example, Sames and Moebs, 1989).

### Deformation Event D1b

During D1b time the stress field changed sufficiently to develop a new shear orientation that, for example, is represented by some of the large shears in the Deep Mine #6 mine (Figure 7 and 13). These shears lie at a mean orientation of  $358, 70$  (Table I). The D1b shear set is oriented with a more northerly strike at about  $33^\circ$  from the earlier D1a set, and steep easterly dips instead of dips to the west, as is the case with D1a faults. Extension fractures associated with the D1b sub-event strike to the northeast and dip steeply to the southeast. New fault segments that developed during D1b time were characterized by oblique normal-sinistral displacement. In addition, the D1a faults were reactivated during D1b time with sinistral-reverse displacement. Although the D1 faults originally penetrated thick layers of sedimentary rocks, now, as a result of displacement and re-annealing of the coal, they and their associated extension fractures commonly terminate at the contact of the coal seam or at other bedding-slip planes in adjacent overlying or underlying sediments (Figure 12).

With D2-event reactivation and offset, a segment of the D1b shear (at arrow, Figure 13) was altered. It appears to “roll over” into the near-orthogonal D2 intra-seam shear and its splay.

As D2 faulting occurred, LA splay faults offset and reactivated the D1 faults, and, where that occurred, the D1 faults appear to abruptly

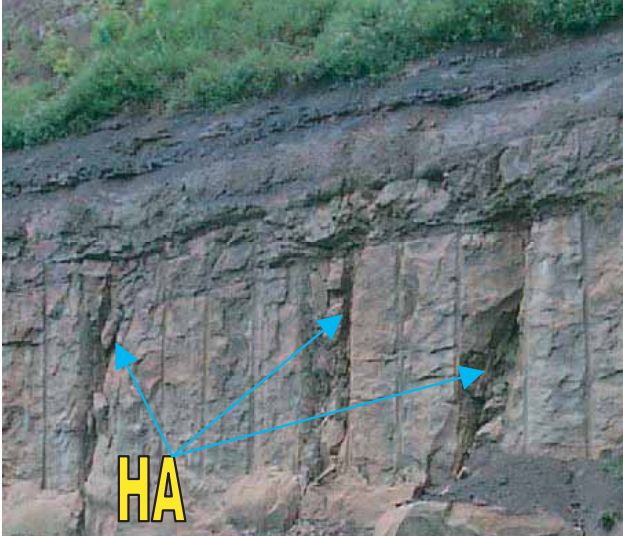


Figure 12. Road cut (State Highway 160) of arenite (brown) overlain by sheared graywacke bed (gray) and coal seam (black). Note that the high-angle fractures (HA) do not cut the highly sheared graywacke or the coal seam.



Figure 13. Cross-section view of fault intersection (Deep Mine #6 mine) of D1b fault at vertical paint line (yellow arrow) with D2 LA intra-seam shears (horizontal paint lines). Overhanging "brow" (upper right quadrant) is perpendicular to "right rib" and its bottom edge is marked by white line. Coal in upper-left quadrant is highly deformed.

change dip by as much as  $90\text{-}100^\circ$  within a distance of about one meter. The interpretation that the two are a single fault is unlikely because of their near-orthogonal orientation, the conjugate-fracture geometries and the kinematic indicators (opposing slickensides).

Sometimes, at these D1 and D2 fault intersections the total thickness of the coal seam is increased by two or three times. The reactivated D1 fault plane acts much like a bulldozer blade "scraping up" and intensely deforming coal in the upper part of the seam in front of the D1 fault. The thickened wedge of coal typically shows obvious tightly folded and sheared coal and wall rock, and rotated blocks rarely with included, polished, coal-coated and folded fragments of arenite or graywacke. Locally, especially where D2 splay faults enter the roof, coal is injected into or coats the surrounding fractures, further weakening the roof rock. The coal-seam thickness at about 3.5 meters in the left half of Figure 13 is over double the thickness of the surrounding seam in the lower-right quadrant and behind the photographer. The "brow" in the upper-right quadrant (between white line and vertical painted line) is slickenside and coal-coated roof rock (see close up in Figure 7).

Sub-event D1b exhibits a slightly different stress field orientation from that of sub-event D1a (Table II and Figure 14). In this case, there is a  $19^\circ$  counterclockwise rotation of the stress axes approximately about the D1a  $\sigma_1$  axis (specifically at 308, 13, right-hand rule). The timing and orientations of both face and butt cleating are consistent with their development as conjugate fracture sets during the D1 event. Poles representing sets of cleating orientations measured throughout the coalfield are clustered in two groups on a stereonet (Figure 15). The two mean cleating orientations are separated by an angle of  $62^\circ$ , and they are similar in orientation to those reported by Milici and Gathright (1982). One group with a mean orientation of 117, 84 (right-hand rule) aligns along the great circle girdle of event D1a indicating it is probably of the same stress field orientation as that of event D1a (for explanation of technique, see Byington, 2003).

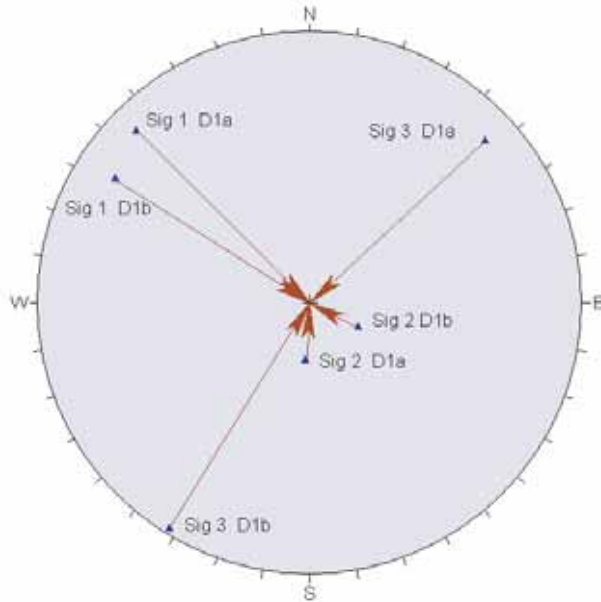


Figure 14. Stereonet plot of mean stress-field axes orientations for deformation sub-events D1a and D1b. (Sigma abbreviated as Sig).

The angle of separation between the main-shear and that of the cleating is  $52^\circ$ .

The second group of cleats with a mean orientation of 67, 83 aligns along the great-circle girdle of event D1b, again suggesting a conjugate relationship and a similar stress field (Figure 15). It also occupies a position that is consistent with the conjugate fault orientation (main-shear-to-cleat-angle of  $68^\circ$ ).

It is important to recognize, however, that cleating is not ubiquitous or even necessarily consistent within a seam. Face, butt or no cleating may dominate in each coal seam, and the frequency of cleating may significantly change within various layers in a seam. At some locations, where the seam has doubled in thickness as a result of duplexing, the upper or lower layer of coal may possess cleating while the opposite layer does not (Figure 16). Typically, these layers are separated by a highly sheared ultracataclasite sole. These are routinely, although incorrectly, called middleman beds, a term which implies a sedimentary rather than tectonic origin.

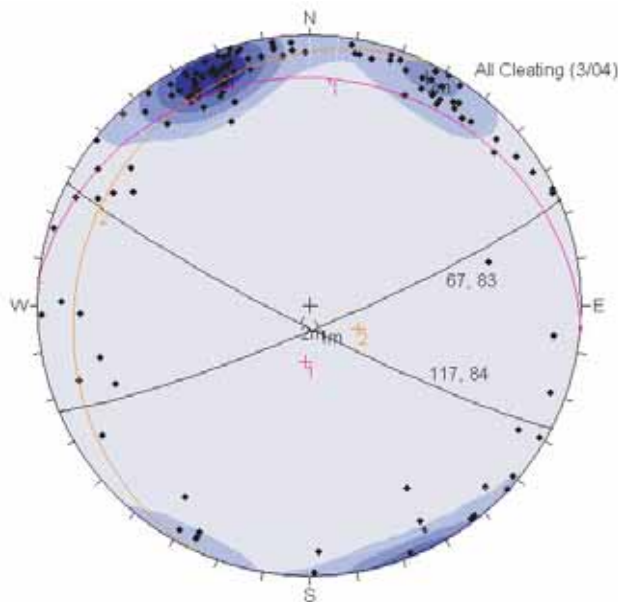


Figure 15. Stereonet plot ( $n = 257$ ) of face- (67, 83) and butt-cleating (117, 84) poles (black diamonds) with representative mean great circle orientations (black arcs). Great circle girdles for deformation sub-events D1a (magenta arc) and D1b (orange arc) are also shown.



Figure 16. Imboden seam (Dorchester #4 mine) with thin well-sheared graywacke duplex sole (below blue pencil). Note strong cleating in the upper coal layer and no cleating in the lower coal layer.

## Deformation Event D2a

### *Semi-ductile domain*

Like event D1, deformation event D2 consists of two separate sub-events, both of which generated new fractures and displacements, and both of which exhibit a unique paleo-stress field orientation. Both D2 events reactivated the earlier D1 event faults and fractures (Table II).

The earliest D2 event (D2a) occurred with a near-vertical  $\sigma_3$  orientation resulting in southeast to northwest horizontal compression of the rock mass and low-angle thrusting (Table II). Figure 17 illustrates the comparative orientations of the three paleo-stress axes for both deformation events.

When compared to Figure 14, it is apparent that during D2a,  $\sigma_1$  rotated approximately  $30^\circ$  (from D1b) to a more northerly bearing. At the same time  $\sigma_2$  and  $\sigma_3$  also rotated a similar amount in a clockwise direction. At this time the kinematics changed from strike-slip dominated to dip-slip dominated. Kinematic indicators, found primarily as conjugate faults, extension fractures and riedel shears, record displacement along thrust faults typically hosted in the coal seam or shale horizons. The calculated slip direction of the upper plate is  $335^\circ$ , indicating the sense of dip-slip displacement was directed toward N25W. As discussed earlier, this displacement and its stress-field orientation are not consistent with the set of folds generated in event D1 (Figure 6c), but are entirely consistent with the folds generated in event D2 (Figure 6d).

The earliest kinematic indicators noted in event D2a consist of various mylonitic features observed in both macroscopic scale and in subsequent petrographic analysis. These ductile faults typically cut the D1 cleating (Figure 18) although infrequent exceptions to this temporal relationship can be found. The mylonites are typically re-annealed, generally with remobilized coal, regardless of whether they are hosted in coal or another type of rock.

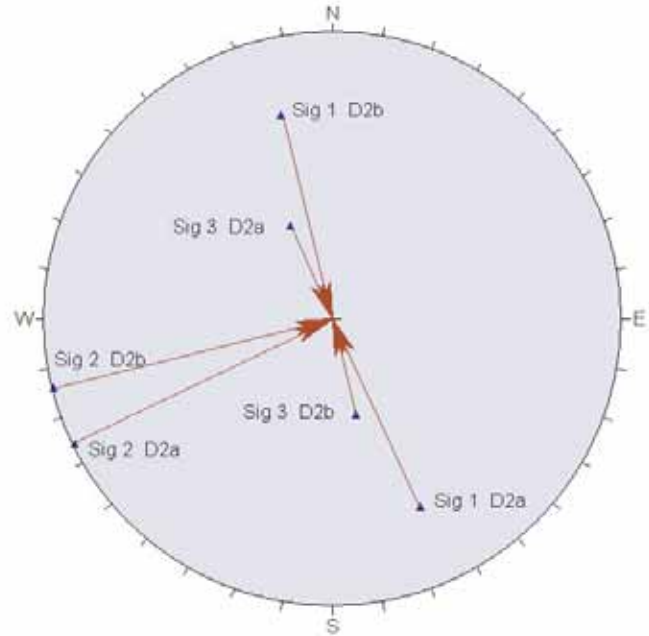


Figure 17. Stereonet plot of mean stress-field axes orientations for deformation sub-events D2a and D2b. Compare the orientations for  $\sigma_1$ ,  $\sigma_2$  and  $\sigma_3$  (shown as Sig 1, Sig 2 and Sig 3) with Figure 15.



Figure 18. Coal seam (State Highway 160) showing orthomylonite-style shearing (highlighted with yellow lines) that cuts coal cleating (vertical) and destroys earlier primary and secondary structural fabrics. Note blue pencil for scale.

Except where destroyed by later brittle faulting, each coal seam contains orthomylonitic flow structure recorded in thin section as included re-annealed and stretched sandy inclusions, stretched cutinite macerals, or as lenticular vitrinite boudins of coal (Figure 19). As a result of the mylonitization, the coal has been reformed so that much of it is optically translucent and details can be viewed with transmitted light under a petrographic microscope.

The mylonitic fabric occurs as thin, wispy, dark lines in the optically re-aligned coal where low recovery rates along internal micro-shears

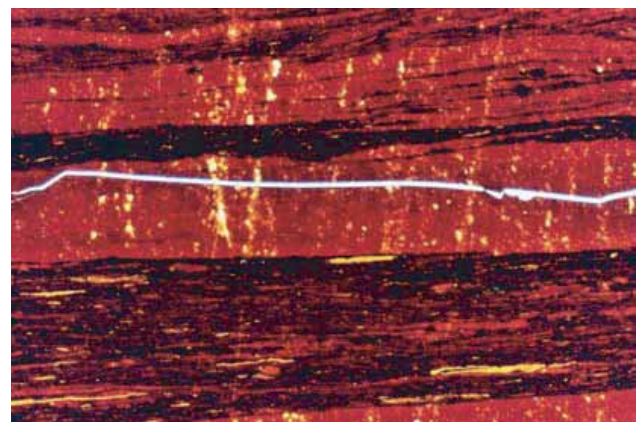
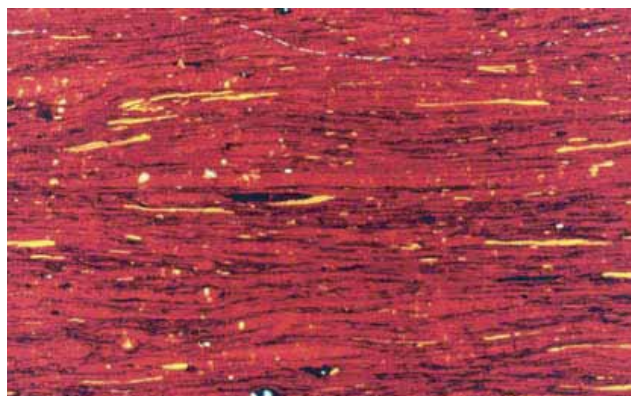


Figure 19. Transmitted-light photomicrograph (crossed polarizer, 0.75 mm field of view) with orthomylonitic fabric in coal showing translucent vitrinite (red) with stretched cutinite macerals (yellow) and opaque micro-shear planes (black streaks). **Upper** – Finely laminated anastomosing micro-shear planes with folded cutinite macerals, and **lower** – alternating bands of vitrinite and bands of micro-shear planes with contained micro-boudins (enclosed red blebs and lenses).

destroy the optical alignment. These dark shear planes form an anastomosing fabric (Figure 19, upper) in the vitrinite, or they occur as distinct dark bands separated by red bands of optically aligned vitrinite (Figure 19, lower). The presence of micro-boudins is also noted within the micro-shear bands. Typically the coal macerals, with the exception of cutinite, have been completely destroyed. Where present, the cutinite macerals are stretched and folded, in some places, around micro-boudins (Figure 20). The micro-boudins may represent lenses of sand grains or they may occur as blebs of re-formed, optically aligned vitrinite. In some cases the cutinite or vitrinite bands are intimately wrapped around or crumpled up against the micro-boudins.

Evidence of mylonitic shear zones is present in the arenite host rock as well. These mylonites are easily identified by their unusual concentration of re-aligned mica grains, and the abundance of anastomosing or well-aligned coal stringers (Figure 21). Typically, many, fine, anastomosing, coal stringers are localized in the mylonite zone. Arenite-hosted zones are contin-

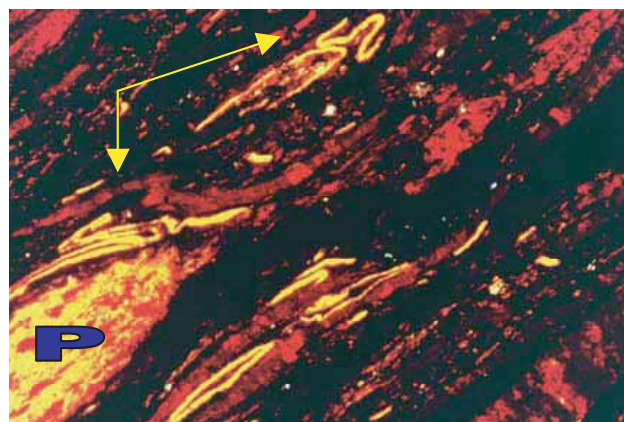


Figure 20. Transmitted-light photomicrograph (crossed polarizer, 0.75 mm field of view) of mylonite fabric in coal seam showing translucent vitrinite (red) with stretched and folded cutinite macerals (thin yellow) and opaque, anastomosing, micro-shear planes (black). Note the folded cutinite and vitrinite (arrows) around the nose of the lensoidal porphyroclast (P).

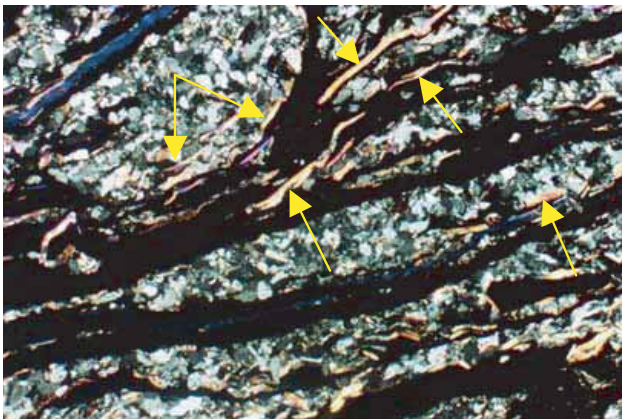
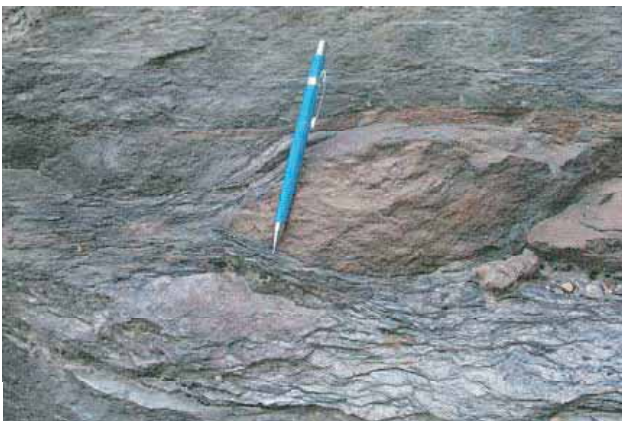
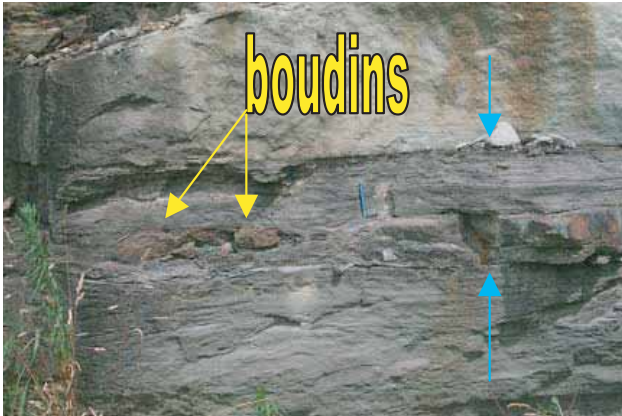


Figure 21. Mylonite zone (Highway 160) in arenite host showing: **Upper** - bedding parallel coal and mica streaked mylonite zone (between blue arrows) with internal sandstone boudins, **Middle** – close-up of local sandstone boudin illustrating the flow foliation, and **Lower** – photomicrograph (crossed polarizer, 0.75 mm field of view) of same mylonitic fabric in arenite showing anastomosing coal stringers (black streaks) and aligned mica (arrows).

uous for many tens of meters in every direction while individual millimeter-thick coal planes can be traced for several meters in every direction.

In rare examples sandstone boudins are enclosed within a ductile shear zone (Figure 21). The boudins locally show strong alignment of the mica grains and may have some foliated carbonaceous fragments enclosed. The coal stringers typically show a distinct anastomosing fabric in both macro- (Figure 21, middle) and microscopic views (Figure 21, lower).

Increased amounts of siderite were commonly noted within the boudins suggesting this compositional variation influences their durability within the core deformation zone. Microscopic examination of sandstone near the mylonitic flow fabric typically reveals undulatory extinction in nearly all quartz grains. In addition, grain size reduction of feldspar framework grains, strict realignment of mica grains and locally abundant coal stringers are also typical of the mylonitic shear zones distal to the coal seam. Arenite-hosted, mylonitic zones containing swarms of narrow coal stringers may oscillate from their shear to their extension orientations. Typically, these swarms of coal stringers continue for tens of meters (Figure 22).

The mylonite zones are characterized by continuous stringers of remobilized coal that are distinctly different from cross bedding, which is typically produced by the alignment of dark heavy-mineral grains. The coal-stringer swarms continue for tens of meters inflecting between two distinct orientations (shear and extension). These swarms are related to the mylonitization rather than to any primary sedimentary feature as is indicated by the lateral continuity of individual coal micro-stringers, their tendency to occur in parallel bands inflecting between two specific orientations, their anastomosing geometry, especially in petrographic analysis, and their common characteristic of cutting through the bedding. In some cases the transition from a haphazard sedimentary orientation of carbonaceous fragments to that of systematic remobilized, shear-induced banding is striking (Figure 23). Where this occurs thin-section petrography confirms that the mica

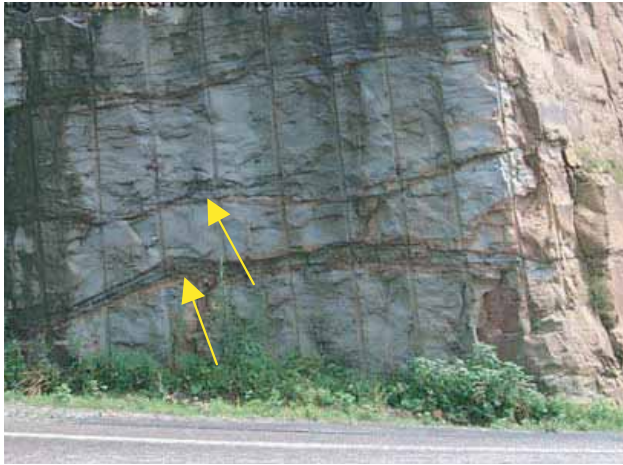


Figure 22. Three coal and mica lined mylonite shears in arenite along State Highway 160 road cut. **Upper** – shears inflect toward extension orientation (left of arrows). **Lower** - close up (lower arrow in upper photo) showing extension orientation of thin coal stringers in shear zone. Note pen point at middle right for scale.

and coal micro-stringers are also well aligned.

Seventeen thin sections of host rock representing nine different surface and underground locations were analyzed quantitatively (Table III). These locations were selected to define the local microscopic structural fabrics, if any. Rock names were based on point count (all >300) analysis for each section. The rock names (modified after Dott, 1964) include carbonaceous graywacke (3), carbonaceous arenite (11) and calcareous arenite (3). The point count analysis of



Figure 23. Reorientation of primary sedimentary carbonaceous fragments (above pencil) to shear-aligned coal stringers (below pencil) in arenite of coal mine roof (Laurel Mountain mine). Well-developed D2 thrust faults occur below rock-bolt plate.

roof rock compositions illustrates the variability in concentrations of diagenetic minerals such as calcite and siderite, and the different concentrations of coal as interstitial blebs and secondary coal stringers.

Concentrations of calcite, occurring almost exclusively as diagenetic cement, range from 0 to 26.7% of the total rock in a carbonaceous arenite and a calcareous arenite, respectively. Concentrations for siderite, occurring almost exclusively as a secondary mineral replacing calcite, framework grains and/or matrix, range from 0.001 to 30.6% of the total rock for a carbonaceous graywacke and a calcareous arenite, respectively. Concentrations of coal stringers range from 2.4 to 43.8% in a calcareous arenite and a carbonaceous arenite, respectively. Concentrations of coal in the form of interstitial blebs range from 1.1 to 14.3% in a carbonaceous arenite and a carbonaceous graywacke, respectively.

A general paragenetic sequence of secondary minerals, excluding clay minerals, was evident from this work. This temporal sequence begins with early diagenetic calcite. With the exception of a few rare calcite framework grains, calcite occurs as diagenetic cement and occasionally as a fracture filling. Only minor local framework-grain replacement is evident in this first-recognized diagenetic phase, and commonly

Table III. Rock composition petrography – showing sample number (ID), number of point counts (No. Points), concentration of quartz (Qtz), mica (Mic), potassium feldspar (K-Fel), calcium feldspar (Plag), calcite cement (Cal), siderite cement (Sid), matrix clay (Clay), carbon in stringers (Str C), carbon in blebs (Bleb C), and matrix (Mtrx).

ID:	No. Points	% Mic	% K-Fel	% Plag	% Cal	% Sid	% Clay	% Str C	% Bleb C	% Mtrx	Total %	
H160 4	319	8.5	3.1	0.01	0.01	0.001	0.001	53.3	26.6	6.3	0.001	97.8
H160 5a	366	27	12.6	13.7	4.4	2.1	8.5	2.7	17.5	5.2	4.9	98.9
H160 5b	363	17	8.5	5.5	1.9	26.7	30.6	0.01	5	4.4	0.3	100.0
H160 5c	338	21	6.5	8.9	3	25.1	30.5	0.01	3	1.2	0.9	99.8
H160 5d	397	18	3.5	9.8	1.8	22.9	17.1	0.8	15.4	8.8	2.3	100
H160 5e	381	18	7.9	10.5	1	2.9	0.5	0.8	43.8	3.4	7.6	96.8
H160 6a	392	30	6.9	15.3	2.8	0.0	3.8	0.01	29.3	3.1	7.9	98.9
H160 6b	407	30	6.1	11.3	1.7	0.7	5.2	0.01	27.8	2.7	6.9	91.9
H160 7	427	42	7.7	14.5	4.7	0.7	3.4	3	12.2	1.6	8.2	98.1
KCT 3	364	46	6.6	12.6	2.7	4.4	6.9	0.01	11	1.1	8.8	99.7
KCT 4a	349	34	8.6	16.3	3.1	1.1	2.3	0.01	26.9	2.6	5.4	99.8
KCT 4b	400	41	3.8	23	2.2	1.5	8	0.8	13.8	1.8	4	100.1
KCT 5a	436	32	11.9	19.3	2.3	0.5	8.3	2.1	16.1	3	4.6	100.2
KCT 5b	335	42	7.8	14.6	2.1	1.8	17.6	1.8	2.4	2.1	8.1	100.1
KCT 5c	342	31	4.1	8.2	1.2	1.2	15.5	0.01	3.8	14.3	21.1	100.1
KCT 6	305	46	9.8	8.5	0.1	1.6	13.8	1	9.5	3.7	6.2	100.1
KCT 7	345	45	6.7	13.9	3.8	2	14.5	1.4	2.6	1.4	8.7	99.9

this occurs as calcite replacing earlier calcite, or in some cases, calcite replacing matrix. Bleb coal of primary sedimentary origin occurs as an interstitial filling (Figure 24). It is not replaced by, but probably antedates, the calcite. Neither the calcite nor the bleb coal shows any obvious association with fractures.

Where present, siderite replaces calcite, the matrix and all framework grains. Siderite commonly, though not always, has a strong spatial correlation with fractures suggesting that the calcite-cemented rock was fractured before the introduction of siderite-depositing fluids. Commonly, bands of siderite blebs occur in a ~0.5 millimeter halo around through-going fractures suggesting that the movement of siderite-depositing fluids may have been facilitated by late (but undefined) fracturing of the host rock.

Finally in the paragenetic sequence, stringers of coal were apparently formed, in part,

by remobilizing interstitial coal. These secondary coal stringers occur in both graywacke (Figure 24, upper) and arenite (Figure 24, lower). These coal stringers follow fractures that cut all other primary and secondary minerals including calcite and siderite. As the anastomosing fracture network is filled with coal, thin slivers of host rock cemented with calcite, or more rarely containing siderite blebs, are isolated and surrounded by coal. These geochemically isolated slivers also document the late formation of the coal stringers. The mica grains exhibit a near perfect parallel alignment with the coal stringers.

The petrographically measured concentrations of each component in the host-rock were compared using non-parametric statistics. All concentration values listed in Table III were included in a spearman-rank correlation matrix (Table IV). Moderate positive correlations between the silicate framework grains and between the two car-

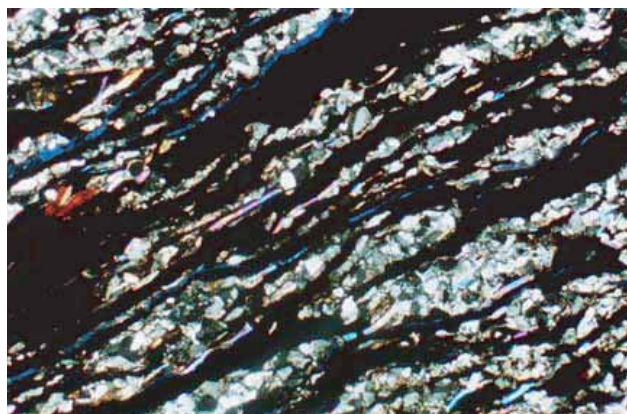
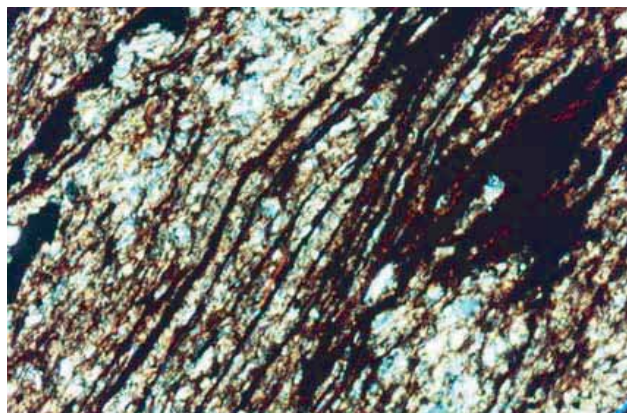


Figure 24. Transmitted-light photomicrograph (crossed polarizer, 0.75 mm field of view) of: **Upper** - graywacke with thin stringers of coal cutting through now-elongated blebs of coal, and **Lower** - arenite with anastomosing stringers of coal cutting through and elongating blebs of coal. All of the slivers of arenite “floating” in the coal are cemented with calcite.

bonate minerals are not unexpected. The moderate negative correlations between bleb carbon and framework grains, but not matrix, suggests that the bleb coal may be more common in graywacke than arenite. The strong negative correlation between siderite and stringer coal suggests that they occupy different fracture sets. It appears that earlier fractures were filled by siderite thereby reducing permeability, and later fractures were filled with remobilized coal.

## Deformation Event D2a

### *Brittle domain*

Following earlier ductile-domain deformation, the coal and surrounding rock was subjected to cataclasis possibly as a result of increased strain rate (probably increased displacement rate) and/or decreased recovery rate (probably pressure and temperature reduction due to unroofing). New brittle-deformation faults and fracture sets developed during event D2, presumably as a result of deformation associated with the Alleghany orogeny, indicate thrust-faulting kinematics.

The D2 thrust faults commonly occupy coal seams (Figure 25) or other weaker rock types such as shale. They are effectively trapped in the weaker horizons and follow them for great distances before inflecting upward. Where this happens, the splay faults play a particularly important role in deforming and weakening the immediate roof rock above the seam.

Where found within the coal seam or at the contacts, the LA D2 faults are herein called intra-seam (IS) shears. They may occur within the coal seam or may occur at the upper or lower contact, and there may be several IS shears within the same seam. They may also occur in the roof rock or may follow rider seams, weakening the proximal host rock.

The IS shears usually are easily differentiated from the surrounding coal by their much more friable composition and sigmoidal fabric (Figure 25, upper). Where the coal can be broken only by hammer blows above and below, the enclosed IS shear breccia commonly can be easily excavated by hand as if it were unconsolidated gravel. The breccia fragments are lensoidal in shape at all scales, and they have shiny, clay- or coal-coated slickensides. When the fragments are broken, successively smaller fragments with slickenside surfaces and lensoidal shape are produced.

One or more of the IS shears are always present within the seam or at the contacts of the

Table IV. Spearman-rank correlation matrix of rock composition (moderate correlations greater than 0.3 and less than 0.5 are shown in green, and correlations greater than 0.5 are in bold red).

	Qtz	Mic	K- Fel	Plag	Cal	Sid	Clay	Str C	Bleb C	Mtrx
Qtz	1.000	0.243	<b>0.483</b>	<b>0.331</b>	-0.171	-0.010	0.084	<b>-0.390</b>	<b>-0.576</b>	<b>0.654</b>
Mic		1.000	0.282	<b>0.319</b>	0.074	0.037	0.173	0.066	-0.017	0.064
K- Fel			1.000	<b>0.596</b>	-0.277	-0.245	0.115	0.179	<b>-0.510</b>	0.235
Plag				1.000	0.113	0.034	0.061	-0.132	<b>-0.576</b>	0.211
Cal					1.000	<b>0.614</b>	<b>-0.427</b>	<b>-0.372</b>	-0.106	-0.102
Sid						1.000	-0.194	<b>-0.775</b>	0.047	-0.110
Clay							1.000	-0.028	0.112	-0.120
Str C								1.000	0.287	-0.196
Bleb C									1.000	-0.294
Mtrx										1.000

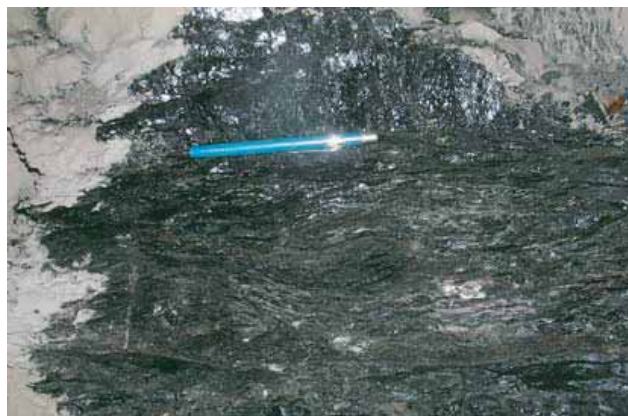


Figure 25. D2 intra-seam shear (below blue pencil, Deep Mine #6 mine). **Upper** – IS shear highlighted by rock dust coating (coating removed at pencil), and **lower** – close-up of rock-dust free zone showing “wavy” anastomosing characteristic of sigmoidal shear fabric.

seam, and as a group they are commonly laterally continuous for kilometers, occurring throughout the entire mining exposure. Frequently, the IS shears are sub-parallel to the bedding and they occupy the contact between the host rock and the coal seam (Figure 26). Typically, in cross section the host rock at the IS shear will have a 10 to 20 centimeter-thick zone of brecciated rock exhibiting a sigmoidal fabric. This occurs as a result of anastomosing shear planes crossing in a pseudo-rhomboidal pattern (Figures 25 and 26).

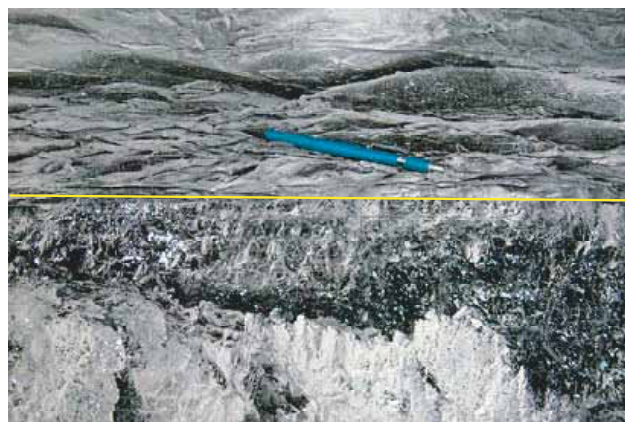


Figure 26. Intra-seam shear occurring above the upper coal seam contact (yellow line) within the Buchanan #1 mine. Note sigmoidal texture in core deformation zone in graywacke host (at pencil).

The LA extension fractures of sub-event D2a are found in all mines and in all coal seams, although at different frequencies. The geometry between the D2a set of extension fractures at N65°E with a 30° inclination to the southeast and their conjugate thrust-fault planes documents reverse kinematics (after Byington, 2003).

Typically these extension fractures are well developed in the roof or floor rocks occurring at dip angles of about 30 degrees. Typically, they occur as narrow swarms several tens of meters wide separated by much wider zones of relatively unfractured rock. As described in Table I, these fractures are planar overall although most commonly they rotate in strike at the fracture tips, resulting in a scalloped trace across the roof (Figure 27). Commonly, these extension fractures are polished, and frequently they are coated with tan or dark brown clay, rock flour, or in some cases, coal.

These LA extension fractures are very important features with respect to roof stability. Their lack of cohesion due to slickensides and coal-, clay-, or rock-flour coatings, results in them being involved, more than any other fracture type, in both small and large roof falls. In mines where the extension fractures associated with the IS shears are abundant, correspondingly greater roof control concerns are experienced. Within the Pocahontas #3 seam, for example, extension

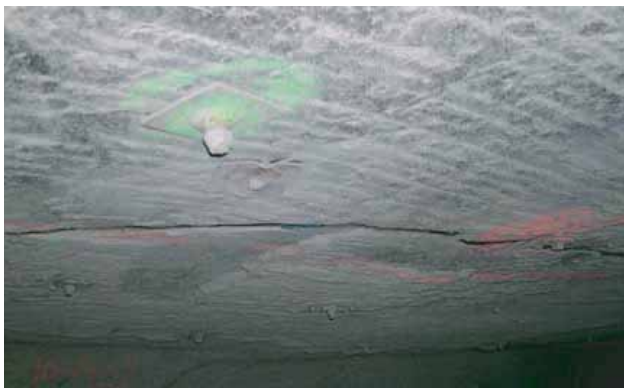


Figure 27. Typical appearance of LA extension fractures in roof (dark line). Fracture is inclined into roof away from viewer at a dip angle of 30°. Note 20-centimeter cable-bolt plate (green) for scale.

fractures and roof fall occurrences are most frequent in a swarm of extension fractures that cuts diagonally across the entries in the Buchanan #1 mine. Elsewhere in this mine and in the adjacent VP8 mine, the roof is not highly fractured, and the roof-fall occurrences are minimal.

Where the roof rock is particularly competent, the IS shears may “stack up” within the seam decreasing their otherwise normal spacing. This phenomena increases the local intensity of deformation in both the coal seam and in the overlying roof rock, especially where the IS splays exit into the roof. The resulting deformation commonly includes displaced wedges of coal (Figure 28, upper), highly deformed, IS shear-bounded sheets (Figure 28, middle), or intricate steeply inclined and commonly-folded duplexed blocks (Figure 28, lower).

Locally this stacking or duplexing of IS shears may significantly increase the total thickness of the seam thereby influencing the mine economics. As the thickness of coal is commonly controlled by this process, predicting where this happens can impact profitability, or may significantly improve exploration success.

As might be expected, the seam is thinned equivalently in the adjacent area from where the coal was removed. In the Raven seam in the Deep Mine #6 (Figure 28, middle), the seam varied from a mean thickness of 1.7 meters to a thickness of ~2.5 meters within a horizontal distance of 5 meters. Continuing the same traverse about fifteen meters farther, the seam thinned to a thickness of ~0.2 meter. Various explanations, sedimentary and otherwise, were considered for this thickening and thinning, but only the tectonic explanation is consistent with the field observations and the stark geometric contrasts in thickness shown by coal-thickness isopach maps.

At some point the “stacked” IS shears exit into the roof, and commonly, where this occurs, they generate particularly unstable roof conditions. Bedding that is nearly horizontal a few meters away may be folded around to dips of 30- to 70-degrees where the IS shears exit into the roof. The folded, and commonly delaminated, bedding planes may be coated with slickensided



Figure 28. Duplexed coal seams. **Upper** – Relatively undisturbed upper coal layer (above yellow line) over folded and sheared (at blue pencil) lower Jawbone seam coal. **Middle** – Overriding layers of coal bounded by IS shear at top, middle (just below pencil) and bottom (not shown) of Raven seam producing local double thickness of coal seam. Note interconnecting riedel shears parallel to pencil (at orange cap light spot). **Lower** – imbricated and folded duplex of Kennedy seam producing 8X increase in thickness.

coal or clay, or may contain stringers or layers of coal.

It is clear that a direct and verifiable relationship exists between “bad” roof conditions and the frequency of fractures associated with IS shearing. Where the intensity of IS shear and conjugate fracture development is minimal, the number of roof falls are negligible, even where significant HA fractures are present. For example at the Mine #1 location in the Splashdam seam, the IS shear is nearly inconspicuous, consisting of one or more narrow glide planes within the coal (Figure 29). The mine workings expose roof rock that has been standing for 20 to 30 years in some currently active entries. Even though this relatively old roof locally has well-developed HA fractures, no evidence of dangerous roof deterioration is apparent.

In one segment of the Splashdam seam a local duplex results in the seam thrusting over itself, and in the process, incorporating a sheared “middleman” graywacke sole. Uncharacteristically, the LA extension fractures are nearly non-existent, and not surprisingly, the roof conditions are excellent.

The IS shears do not present any significant roof-control problem when they are oriented near parallel to bedding. However, when they begin to diverge in dip from the bedding they significantly affect the thickness and strength of the coal seam (Figure 28, upper and middle). Com-



Figure 29. IS shears (horizontal brown lines) characterized by narrow glide plane and almost no conjugate extension fractures in roof.

monly, where they exit into the roof, splays of the IS shears also drag coal from the seam into the roof where they leave the seam (Figure 30, upper and middle).

These wedges of coal quickly taper down in thickness within two or three meters. However, the coal-coated and slickensided fractures are carried many tens of meters into the roof. In the Imboden, Raven and Jawbone seams, many ground falls are directly associated with splay faults that “drag” coal into the roof, decrease the cohesion of, and fold and fracture the roof rock.

Where the IS splays do not “drag” coal into the roof, they commonly create zones with high fracture densities that are commonly associated with roof falls (Figure 30, lower). Commonly, these slip planes cross but do not reorient bedding and they are frequently coated with clayey gouge. This gouge commonly maintains some cohesion initially, but it may lose that cohesion later as dehydration occurs as a result of exposure to mine ventilation.

In addition to the larger splay wedges the roof may be penetrated with ~1-centimeter-thick stringers of coal that cross bedding at acute angles (Figure 31). Commonly, these stringers narrow within a few meters, but, as was the case with the larger splay wedges, the coal-coated fractures commonly continue for many tens of meters into the roof strata. This virtually cohesionless discontinuity is commonly found as a bounding wall on some of the largest roof falls.

In many other instances the coal appears to have been injected into the roof rock (Figures 8 and 32). The coal contact at these locations is typically very angular, and does not necessarily exhibit planar geometry, and the contacts may be quite irregular. These discontinuities, like those described above, significantly change the mechanical characteristics of the host rock.

### Deformation Event D2b

Sub-event D2b developed extension fractures along with the IS shears. They are very similar in all characteristics to D2a extension fractures with the exception of their opposing-

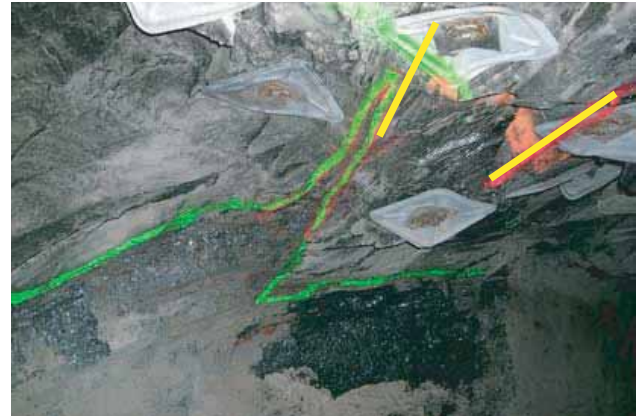


Figure 30. IS shear splays exiting coal seam into roof strata near roof falls. **Upper** – IS splay (Raven seam) exiting into roof arenite and “dragging” coal along with it (green paint along coal/host contact). Yellow lines indicate local bedding dip, which otherwise is near horizontal 10 meters in either direction perpendicular to bedding strike. **Middle** – Coal wedge (inside orange paint) cutting sandstone roof rock above near-horizontal main coal seam (lowest paint line). **Lower** – Highly fractured roof associated with IS splay fault exiting into roof (Jawbone seam).

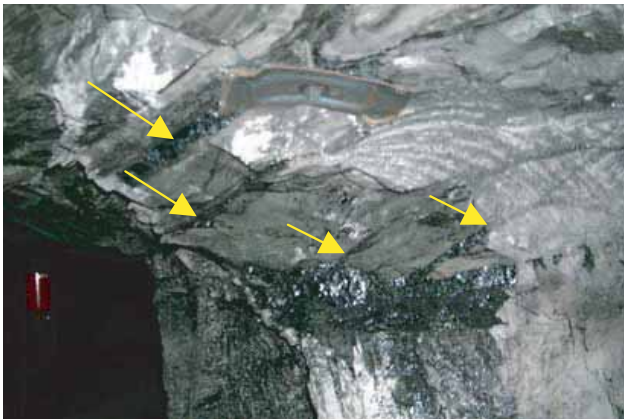
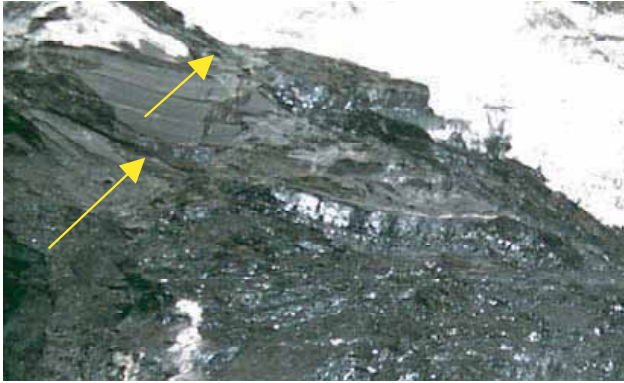


Figure 31. Coal-stringer-filled extension fractures cutting bedding (at arrows). **Upper** –Raven seam. **Middle** –Jawbone seam. **Lower** – Imboden seam.

dip orientation. They also typically terminate at the earlier D1a, D1b or D2a extension fractures, although in lieu of D1 or D2a extension fractures, they continue for meters into the roof strata.

When all of the LA fractures associated with events D2a and D2b are plotted on a stereonet, two distinct extension fracture groups are



Figure 32. Coal stringers showing angular contacts resulting from injection into sandstone host.

easily discernable for each of the mines. Commonly, the more frequently measured fractures represent the earlier D2a thrusting. The less frequent set consists of kinematic representations of the subsequent D2b normal displacement. That the D2b sub-event followed the main D2a sub-event is clear, but it is not clear if this happened as two entirely separate sub-events or as multiple repeated actions of incremental stick-slip of reverse displacement followed by normal relaxation. In other words, there may have been a period, or many periods, of normal relaxation that followed each period, or many periods, of thrusting. The early reverse displacement moved the upper plates along a mean orientation of N45°W whereas the normal relaxation moved the upper plates along a mean orientation of S25°E. This 160° difference in bearing suggests that the rock

mass moved in a zigzag pattern of displacement.

Where the two opposing LA extension-fracture sets intersect, the chance of roof falls is greatly increased. In fact, pyramidal-shaped blocks called “horse backs” (Figure 33) often fall from the roof during initial mining or shortly thereafter. These D2a and D2b extension-fracture-bounded fall blocks are typically in the range of several tons in size. Where they intersect the HA extension fractures, the fall blocks are typically an order of magnitude larger. For this reason alone, it is important to consider both fracture types and their orientations when considering the optimal roof support methodology and the optimal workings orientation (Byington, 2004).

The same extension fractures described above are also found associated with floor buckling and heaving (Figure 34). In places where buckling occurs in the floor, it almost always is associated with clay-coated smooth extension fractures identical to the ones found in the roof. Therefore, as might be expected, floor buckling typically occurs in discrete zones similar to those typical of roof falls, although they seldom will occur adjacent to one another because of the IS shear displacement discussed previously. They are typically far less conspicuous because they are covered with dust and broken rock.

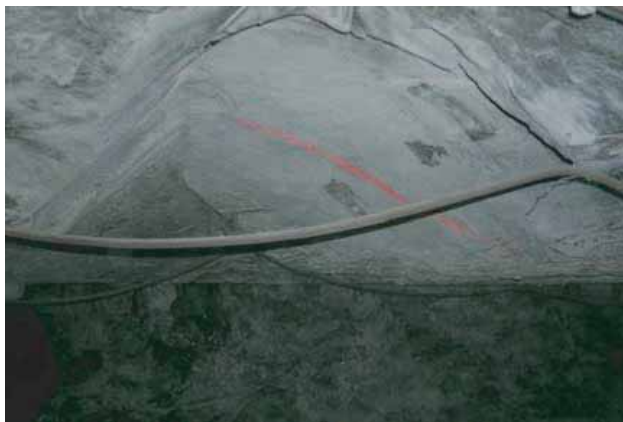


Figure 33. Pyramidal void (“horse-back” void) caused by intersecting extension fractures of sub-events D2a and D2b.



Figure 34. Floor buckling along LA extension fracture. Fracture is polished and clay lined. Note hammer for scale.

Because of displacement along the IS shears, variations in the fracture density between the roof and floor may be considerable. The accommodation of strain may occur as buckling in places where significant strain shortening occurs in the roof. Reorienting the workings as described by Byington (2004) can significantly reduce the occurrences of roof falls and floor buckling.

### Other Tectonic-related Discontinuities

Uniaxial Compressive Strength (UCS) rock-strength testing (Mark and Molinda, 2003) confirms that bedding composition discontinuities can significantly affect the strength of the rock along those discontinuities. The bedding parallel or diametral strength of coal-stringer-bearing roof rock may be as little as one-sixth of the axial strength, and typically approximates one-third of the axial strength of host rock (Molinda and Mark, 1996). Bugden and Cassie (2003) also found that the UCS was significantly reduced by as much as 90% of UCS axial strength when failure was initiated along bedding in well-bedded strata such as shale. They found the UCS was only slightly reduced when bedding failure occurred in a poorly bedded, coarser-grained strata such as sandstone.

The anastomosing fabric typical of shearing indicates that, as the micro-shearing pen-

erates the rock, the interstitial coal blebs are stretched into elongate stringers, and at the same time displacement along micro-shear planes rotates and reorients individual mica grains so that they parallel the micro-stringers (Figure 24 and 35). The presence of calcite cement within all of the completely enclosed “floating” slivers of arenite or graywacke suggests that this happened after the introduction of diagenetic calcite-cement.

Delamination of coal-mine roof rocks is invariably found in the mines along compositional discontinuities related to high concentrations of coal stringers, realigned mica and/or clay horizons. Dark bands occurring as bedding-parallel concentrations may contain more than 50% coal (Figure 35 upper), which, without detailed microscopic inspection, may appear to be a primary sedimentary features. However, when viewed in thin section (Figure 35 middle), it is apparent that the coal stringers connect with each other in a sigmoidal or anastomosing pattern, and they are laterally continuous along strike and cut bedding at acute angles.

With a horizontal (discontinuity-parallel) orientation of  $\sigma_{10}$ , delamination occurs in all rock types containing coal micro-stringers, aligned mica grains or clay discontinuities (Figure 24 and 35). To aid in identifying the orientation and frequency of these delamination planes, all of the thin sections were resin impregnated. The resulting dark blue streaks of resin indicate where fractures developed as a result of delamination. These delamination fractures are typically found at the contact between the coal micro-stringers and the host rock.

The formation of coal micro-stringers from hydrocarbon blebs, now coal, is wide spread and apparent in thin section (Figure 36). The syndepositional blebs are apparently mobilized into adjacent post-depositional fractures thereby filling the fractures with coal. This process is similar in appearance to remobilization of petroleum hydrocarbons in younger arenites and graywackes associated with petroleum reservoirs (Byington, 2003, p. 94).

Where delamination occurs along mi-

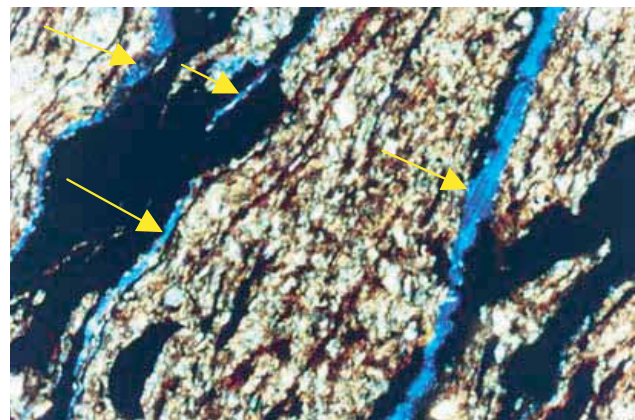
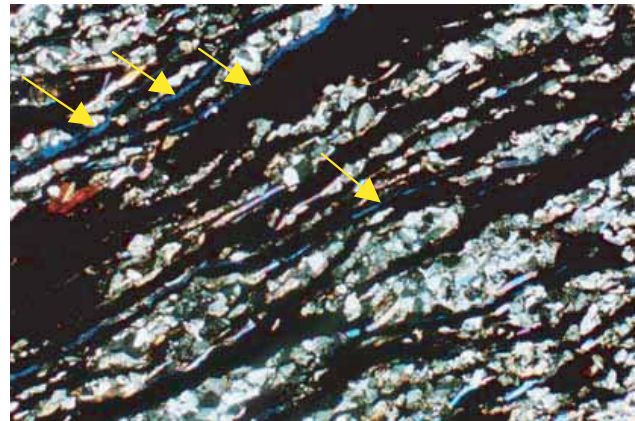


Figure 35. Bands of coal micro-stringers in arenite host (**upper**). Transmitted light photomicrographs (crossed polarizer, 0.75 mm field of view) showing anastomosing coal stringers in arenite (middle), and in graywacke (lower). Deep blue streaks at the coal/host rock contacts are open fracture delaminations (at arrows).

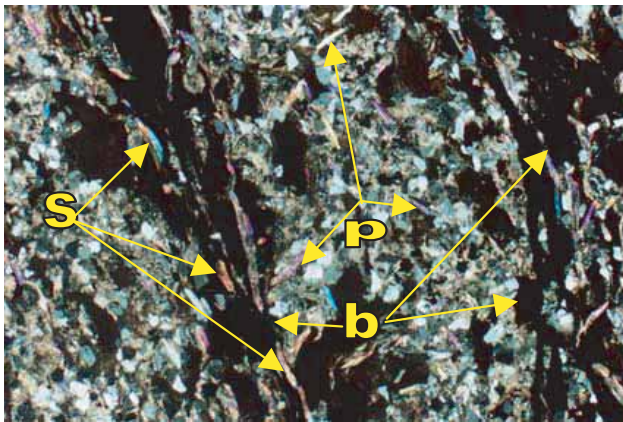
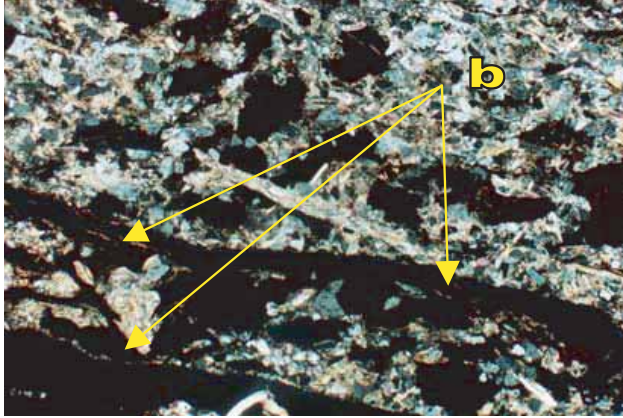


Figure 36. Transmitted light photomicrograph (crossed polarizer, 0.75 mm field of view) showing anastomosing coal stringers and blebs (black) in arenite. **Upper and lower** – stringers cutting and locally remobilizing pre-existing coal blebs (b). **Lower** - primary mica grain orientations (p) have been realigned (s) resulting from shearing directly adjacent to the fractures.

caceous, argillaceous and/or carbonaceous discontinuities, the competency of the roof rock is locally significantly reduced (Figure 37). The effects of delamination are commonly apparent in roof exposures as the separation of beds, and “flaking” of thin layers in the roof.

The coal-stringer and mica laminations in the roof rock are easily identified when the roof strata are well exposed. Commonly, however, the effects of progressive delamination are manifested only after a roof fall has occurred (Figure 38).



Figure 37. Roof-rock delamination along carbonaceous and micaceous micro-shear planes. Rock bolt plates for scale are 20 centimeters.

The fall rock, in a roof fall where delamination has played an important role, displays a very tabular nature in many of the fall blocks. Typically, within individual tabular fall blocks there are wispy black streaks of coal-filled micro-stringers. The tabular surfaces on the top and bottom of the blocks are typically black from the coal and commonly, they also have an abundance of sub-parallel mica flakes.



Figure 38. Roof fall with tabular blocks indicative of roof delamination. Note the fine coal micro-stringer laminations evident as black, wispy, anastomosing fabric (arrow) in very tabular block.

## SUMMARY AND CONCLUSIONS

Fractures are unquestionably the most important component in roof falls, floor heaves and rib spalling. That they are partly responsible for the roof falls is illustrated by large and small falls with planar-fracture bounded blocks in the fall pile and standing walls having at least one smooth planar surface that terminated the fall propagation. However, fractures and weakness discontinuities in the host rock are rarely discussed in the literature, and, when they are, they are typically given an equal standing with various other primary sedimentary features or with diagenetic alteration of the host rock, for example.

A field-based definition of the fracture types, framed within their prehistorical and mining-induced kinematic interactions with each other, is discussed here. The insight provided is discussed within the context of their genesis and deformational history. The model presented prioritizes the fracture types with respect to coal mine roof falls. The fracture types are defined and prioritized within the environment of the typical near-horizontal stress-field orientations recently calculated for mines in the coal field of Southwestern Virginia.

A macroscopic model easily applied in the field is presented whereby weakness discontinuities in the host rock can be recognized. The model recognizes two distinctly different deformation events, which produced four distinct conjugate sets of fractures. Each of these fracture sets can become the primary components controlling roof falls. However, rarely is only one set involved.

Fracture geometries were utilized in defining the paleo-stress fields. From these fracture geometries, the paleo-stress fields associated with four deformation sub-events were calculated. The kinematic aspects were defined for each deformation event and for two sub-events within each deformation event. The paleo-kinematics and paleo-stress fields were calculated independently of other data such as geological mapping

by previous authors, although the calculated results correlate well with the reported mapped displacements along the D1 and D2 faults. The direction of displacement was also calculated for earlier sub-event's fractures as they were reactivated by later sub-events.

It is apparent that the paleo-displacement on the earliest faults began with early sinistral strike-slip displacement with a reverse component. This was followed by oblique sinistral displacement with a small reverse component until, in the final event, the D1a faults were reactivated with dextral displacement, also with a reverse component. The cleating found in most of the seams is related to this earliest deformation event.

Strike-slip faulting of event D1 was followed by thrusting of event D2, presumably related to the Alleghany orogeny. The coal and arenite host record early D2 shearing. The considerable variation in mylonitic versus cataclastic deformation suggests a deformation history that extends over a large range of temperatures, and/or displacement-versus-recovery rates. The D2 faults were dominated by reverse displacement, but there was also subsequent normal displacement on these faults. Brittle faulting followed the early ductile faulting in the coal and host rock.

The LA faults are typically found within the coal seam, being temporarily "trapped" in the seam, or in the graywacke host rock. This, in both cases, most commonly occurs as a result of the much-reduced strength of the coal and graywacke when compared to the surrounding sandstone or graywacke. The individual IS shears can be traced for hundreds to thousands of meters within the seam, and typically one or two IS shears are always present within the seams.

Some of the microscopic rock textures, particularly the mylonitic texture of the coal seams, indicate that the tectonic history of the rock is diverse in tectonic style, and in post-diagenetic paragenesis. Petrographic evaluations and statistical analysis of a limited number of transmitted-light thin sections suggest that the most obvious paragenetic features include an early cementing of sand and silt sized frame-

work grains by calcite cement. The matrix may have been replaced minimally by calcite within the graywacke. Subsequent to this, the rock was penetrated by micro-shears that transported fluids, presumably connate waters, along the micro-fractures. As a result siderite was deposited along the micro-fractures replacing the calcite, matrix and silicate framework grains. Following this, new fractures were initiated and some of the older siderite-related fractures were re-utilized as hydrocarbon (now coal) blebs were remobilized into micro-stringers.

The first of the recognized deformation events produced steeply dipping faults and fractures that were responsible for significant amounts of strike-slip displacement. This event also produced medium-scale folds.

The HA fractures are typically oriented nearly perpendicular to the contemporary stress field, and as such they are tightly closed and are typically more difficult to recognize in the mine roof than those of the LA set. When occurring alone, these HA fractures are very rarely involved in roof falls, but, when found in close spatial association with the LA fracture sets and/or with significant roof delamination, their interaction with the LA fracture sets is commonly responsible for increasing the size and frequency of the roof falls.

The D2 LA fractures are the most obvious and also the most frequent fractures in the mine roof and floor rock. They are genetically associated with regional thrusting and large-scale folding. These shallow dipping fractures are the ones responsible for most of the roof falls. They are an especially common component of the smaller falls. When combined with a near-horizontal  $\sigma_{10}$ , HA fractures and a host rock with abundant and laterally continuous carbonaceous, micaceous, or argillaceous laminations, the LA fractures often become part of medium to large sized roof falls.

Carbonaceous and micaceous laminations in the roof rock are important with respect to roof falls. These discontinuities begin to separate even as the excavation is being made. The very significant changes in rock-strength associated with carbonaceous, micaceous or argillaceous

discontinuities, makes their recognition and consideration in any roof control program imperative. An abundance of near-horizontal coal stringers or tectonically re-aligned mica zones in the host rock, combined with a near-horizontal  $\sigma_{10}$ -  $\sigma_{20}$  plane, can seldom be ignored without serious consequences.

Although relatively easy to discover in the roof rocks, these weakness laminations are apparently rarely factored into the mine roof control programs discussed by other workers. Rider seams can commonly be discovered by a three-dimensional inspection of the roof, but the microscopic discontinuities require a different technique. For example, even with a stratascope examination of the roof rock by qualified inspectors, the microscopic coal and mica discontinuities in the roof are not identifiable. Recognizing the tabular nature of fall blocks, slabby delamination of the roof strata, or distinguishing the wispy or streaky laminations of tectonically induced coal micro-stringers in the roof rock is necessary for identification of potentially dangerous delamination textures.

## REFERENCES CITED

- Anderson, E.M., 1951, The dynamics of faulting: 2nd ed., Edinburg, Oliver and Boyd, 206 p.
- Barton, N., 1976, The shear strength of rock and rock joints: abstract International Journal of Rock Mechanics, Mineral Sciences and Geomechanics, # 13, p. 1-24.
- Bates, R. L., 1936, The Big A Mountain area, Virginia: Virginia Geological Survey Bulletin 46-M, p. 167-204.
- Billings, M.D., 1972, Structural geology: Prentice-Hall, Englewood Cliffs, New J., p. 168-169.
- Bugden, A., Cassie, J., 2003, Tensile roof failure arising from horizontal compressive stress and geological slips, in Peng, S.S., Mark, C., Khair, A.W., Heasley, K., eds., Proceedings 22nd International Conference on Ground Control in Mining: , p 195-202.

- Byington, C.B., 2003, An integrated structural analysis defining structural and geochemical controls of petroleum migration near the 38 and 44 fault systems in the Midway-Sunset Oil Field, Kern County, California: MS Thesis, University of California, Bakersfield, 169 p.
- Byington, C.B., 2004, SOMA: A new method to calculate the operative stress field: Results from the Laurel Mountain mine, Russell County., Virginia, *in* Peng, S.S., Mark, C., Khair, A.W., Heasley, K., eds. Proceedings 23rd International Conference on Ground Control in Mining: , p. 103-111. Also at: <http://www.mme.state.va.us/Dm/SOMA.htm>
- Byington, C.B., Cox, A.D., and Wilcinski, A.G., 1989, The Ivanpah Project of the Mojave Gold province - A structural approach: The California Desert Mineral Symposium
- Byington, C.B., and Russell, M.R., 2001, Economic geology and ore controls of the Santa Rosa Mine: An integrated structural analysis approach, Cañazas, Veraguas, Republic of Panama, *in* Albinson, T., and Nelson, C.E., eds., New discoveries in Mexico and Central America: Special Publication 8, Economic Geology, p. 317-329.
- Compendium: United States Department of the Interior, Bureau of Land Management, California State Office, Sacramento, California, p. 113-124.
- Caddey, S.W., and Byington, C.B., 1988, Ore controls of the Bulldog silver mine, district application and discovery of the Northern Amethyst silver/gold deposit, Creede Mining District, Colorado: AIME Vail Meeting Abstracts, 1988.
- Cloos, E., 1932, "Feather joints" as indicators of the direction of movements on faults, thrusts, joints and magmatic contacts: *Geology*, v. 18, p. 387-395.
- Diederichs, M. S. and Hoek, E., 1998, DIPS – Version 5.1: University of Toronto
- Diffenbach, R.N., 1988, Geology of the Virginia portion of the Clintwood and Jenkins East quadrangles, Virginia: Virginia Division of Mineral Resources Publication 86, 1 p.
- Dott, R.H., 1964, Wacke, graywacke and matrix – an approach to immature sandstone classification: *Journal of Sedimentary Petrology*, v. 34, p. 625-632.
- Engelder, J. T., 1974, Cataclasis and the generation of fault gouge: *Geological Society of America Bulletin*, v. 85, p. 1515-1522.
- Englund, K. J., 1961, Rotational block of the Cumberland overthrust sheet in Southeastern Kentucky and Northeastern Tennessee: U.S. Geological Survey Professional Paper 424, p C74 – C76.
- Harding, T.P. and Lowell, J.D., 1979, Structural styles, their plate-tectonic habitats, and hydrocarbon traps in petroleum provinces: *AAPG Bulletin*, v. 63, p. 1016-1058.
- Harding, T.P. and Wickham, J.S., 1988, State of stress near the San Andreas fault; implications for wrench tectonics: *Geology*, v. 16., p. 1151-1153.
- Henika, W.S., 1989, Geology of the Haysi quadrangle, Virginia: Virginia Division of Mineral Resources Publication 91, 1 p.
- Henika, W. S., 1994, Internal structure of the coal bearing portion of the Cumberland Overthrust Block in Southwestern Virginia and adjoining areas, *in* *Geology and mineral resources of the Southwestern Virginia Coalfield: Virginia Division of Mineral Resources Publication 131*, p.100-120.
- Hoek, E., 2000, Practical rock engineering, 2000 Edition, *at* [www.roscience.com/hoek/PracticalRockEngineering.asp](http://www.roscience.com/hoek/PracticalRockEngineering.asp), p. 313.
- Mark, C., and Molinda, G. M., 2003, The Coal Mine Roof Rating in mining engineering practice, *in* Coal Operators' Conference; p. 252-260.
- McKinstry, H.E., 1948, Mining geology: New Jersey, Prentice-Hall, Inc., p. 290-327.
- McLoughlin, T.F., 1986, Explanation of the Regional Tectonic Map of the Southwestern Coalfield of Virginia: Mine Safety and Health Administration, IR 1177, 17 p.
- Milici, R.C., and Gathright, T.M., 1982, Geologic features related to coal mine roof falls - a guide for miner training: Virginia Division of Mineral Resources Publication 56, 13 p.
- Molinda, G.M., and Ingram, D.K., 1989, Effects of structural faults on ground control in selected coal mines in Southwestern Virginia: U.S.B.M. Report of Investigations No. 9289, 25 p.
- Molinda, G.M., and Mark, C., 1996, Rating the strength of coal mine roof rocks: U.S.B.M. IC 9387, 36 p.

- Molinda, G.M., Mark, C., and Dolinar, D.R., 2000, Assessing coal mine roof stability through roof fall analysis, *in* Mark, C., Dolinar, D.R., and Tuchman, R., eds., *New technology for coal mine roof supports: Proceedings NIOSH Open Industry Briefing*, NIOSH IC 9453, p. 53-72.
- Nolde, J.E., Mitchell, M.L., and Polzin J.K., 1984, Geology of the Prater and Vansant quadrangles, Virginia: Virginia Division of Mineral Resources Publication 52, 29 p.
- Nolde, J.E., Whitlock, W.W. and Lovett, J.A., 1988, Geology of the Pound and Caney Ridge quadrangles, Virginia: Virginia Division of Mineral Resources Publication 84, 8 p.
- Polysos, N., Brandt, K., and Peters, S., 2003, Geotechnical planning basis for the optimization of workings, *in* Peng, S.S., Mark, C., Khair, A.W., Heasley, K., eds., *Proceedings 22nd International Conference on Ground Control in Mining*: p. 186-94.
- Ragan, D.M., 1973, *Structural geology, An introduction to geometrical techniques*: John Wiley and Sons, 2<sup>nd</sup> ed., 208 p.
- Ramsay, J.G., 1980, Shear zone geometry; A review: *Journal of Structural Geology*, v. 2, no. 1, p. 83-99.
- Reid, R.R., Caddey, S.W., and Rankin, J.W., 1975, Primary refraction control of ore shoots, with examples from the Coeur d'Alene district, Idaho: *Economic Geology*, v. 70, p. 1050-1061.
- Sames, G.P. and Moebis, N.N., 1989, Hillseam geology and roof instability near outcrop in Eastern Kentucky drift mines: U.S. Bureau of Mines, Report of Investigation 9267, 32 p.
- Sibson, R.H., 1977, Fault rocks and fault mechanisms: *Journal of the Geological Society of London*, 133, p. 191-213.
- Sibson, R.H., 1989, Structure and mechanics of fault zones in relation to fault-hosted mineralization: Australian Mineral Foundation, Adelaide, Australia, 66 p.
- Sylvester, A.G., 1988, Strike-slip faults: *Geological Society of America Bulletin*, v. 100, p. 1666-1703.
- Tchalenko, J.S., 1970, Similarities between shear zones of different magnitudes: *Geological Society of America Bulletin*, v. 81, p. 41-66.
- Twiss, R.J., and Moores, E.M., 1992, *Structural geology*: W. H. Freeman and Company, New York, New York, 532 p.
- Whitlock, W.W., Lovett, J.A. and Diffenbach, R.N., 1988, Geology of the Wise quadrangle and the coal-bearing portion of the Fort Blackmore quadrangle, Virginia: Virginia Division of Mineral Resources Publication 80, 1 p.
- Wilcox, R.E., Harding, T.P., and Seely, D.R., 1973, Basic wrench tectonics: *American Association Petroleum Geologists Bulletin*, v. 57, no. 1, p. 74-96.
- Wise, D.U., Dunn, D.E., Engelder, J.T., Geiser, P.A., Hatcher, R.D., Kish, S.A., Odom, A.L., and Schamel, S., 1984, Fault-related rocks; suggestions for terminology: *Geology*, v. 12, p. 391-94.
- Xu, J., Qian, M., and Yu, H., 2003, The characteristics of mining-induced fractures in overlying strata, *in* Peng, S.S., Mark, C., Khair, A.W., Heasley, K., eds., *Proceedings 22nd International Conference on Ground Control in Mining*: p. 44-47.

VIRGINIA DIVISION OF MINERAL RESOURCES-- OPEN-FILE REPORT 07-01 --THE TECTONIC HISTORY AND  
CHARACTERISTICS OF FRACTURE SYSTEMS AFFECTING COAL MINE ROOF STABILITY  
IN SOUTHWEST VIRGINIA--2007